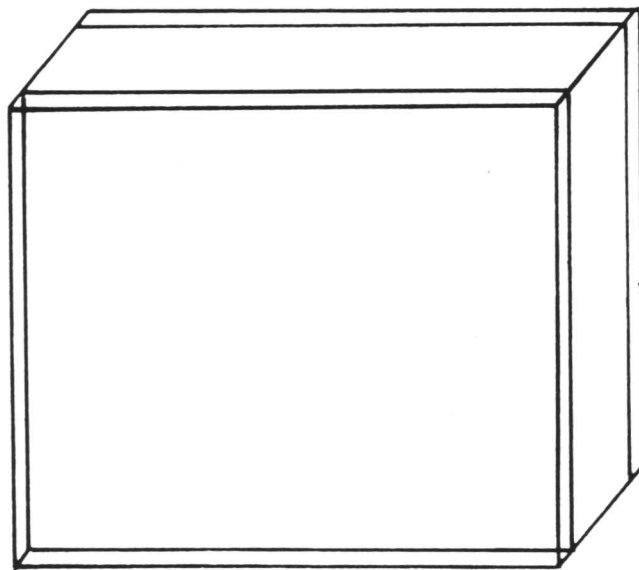


(a)



(b)

Fig. 2.3: Schematic diagram showing the model for one dimensional carbon diffusion-controlled growth of austenite [after Yang, 1988].

2.3 Crystallography of Austenite

Watanabe *et al.* [1975] found that each austenite grain which has been formed from ferrite laths with the same orientation and the austenite has the K-S orientation relationship with the ferrite. Both lath boundaries and cementite play an important role in the formation of austenite grains, with same orientation. When austenite is formed adjacent to precipitated cementite on the boundary, the austenite must have Pitsch orientation relationship with cementite and K-S orientation relationship with ferrite. Lenel *et al.* [1984] have shown that the grain boundary nucleated austenite shows a Kurdjumov-Sachs orientation relationship with one or both ferrite grains on either side of the grain. The orientation relationship between acicular austenite and martensite matrix has been reported to represent the Kurdjumov-Sachs orientation relationship [Matsuda and Okamura, 1974].

2.4 Effect of Heating Rate on Reaustenitisation

The heat treatment conditions can also influence the morphology of austenite. Acicular austenite seems to be inherited from the elongated nature of the prior martensitic laths and/or packets and is formed by slow heating rates and low austenitisation temperatures. Globular austenite appears favoured by the opposite conditions to those described above [Law and Edmonds, 1980]. Kinoshita *et al.* [1974] studied the effect of heating rate in the range of $2\text{ }^{\circ}\text{C min}^{-1}$ to $2\text{ }^{\circ}\text{C s}^{-1}$ from ferrite-pearlite and martensite initial microstructures. They found that heating of ferrite-pearlite at either heating rate gives rise to the nucleation of austenite at ferrite-pearlite interfaces and pearlite colony boundaries. They also indicated that heating of martensite at $2\text{ }^{\circ}\text{C s}^{-1}$ produces a smaller amount of acicular austenite and a large amount of granular austenite at prior austenite grain boundaries. Slow heating of martensite at $2\text{ }^{\circ}\text{C min}^{-1}$ however, produced a large amount of acicular austenite in the prior austenite grain interior along with globular one at the boundaries, which comes to compose a lamellar structure of austenite and acicular ferrite. Law and Edmonds, [1980] shows that as the heating rate was lowered the distribution of austenite nuclei become concentrated around the prior austenite grain boundaries in the martensite and bainitic structures and the ferrite grain boundaries in the ferrite structures. At very low heating rates, the growth of austenite tended to be allotriomorphic, even in the martensite and bainitic microstructures. Yang *et al.* [1990] studied the effect of heating rates on the reaustenitisation from martensitic microstructure in Fe-C-Si-Mn alloy. They found that the transformation start temperature is raised as the heating rate increased (Fig. 2.4).

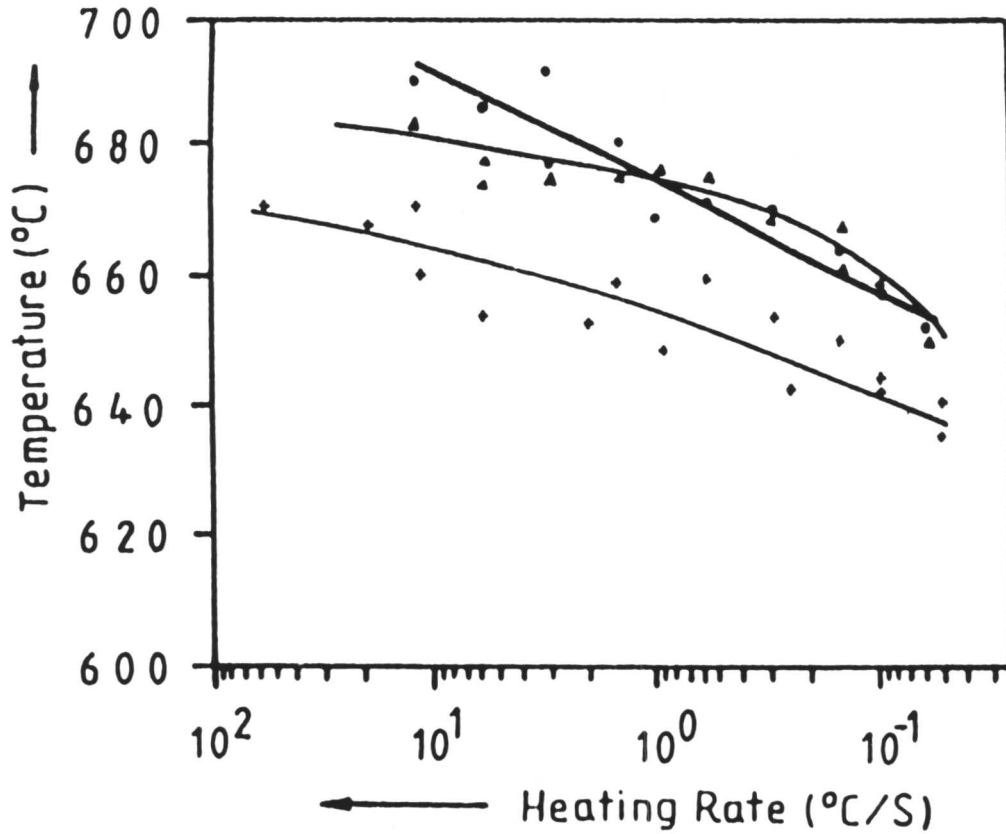


Fig. 2.4: Effect of heating rate on the austenite formation-start temperature during continuous heating in homogenised Fe-C-Si-Mn-Ni weld deposits [after Yang 1987].

2.5 Effect of Alloying Elements on the Morphology of Austenite

The strength and ductility shown by dual phase steels are dependent upon the relative proportions of martensite and fine grained ferrite; the alloy will be stronger but less ductile if a larger percentage of martensite is present in the structure. The percentage of martensite in the dual phase structure will be dependent upon; (a) the carbon content, (b) the annealing temperature, and (c) the hardenability of the austenite region.

Plichta *et al.* [1974] have studied the effect of alloying elements on the formation of austenite by classifying alloy systems into different groups according to the observed morphologies of austenite. They concluded that it is a competition between the nucleation and growth of austenite at lath boundaries and the migration of these boundaries which determine the shape of the final product. However, their

explanations are inconclusive. For example, they have not recognised the effect of alloying element concentrations on the morphology of austenite thus formed. An ‘acicular’ austenite morphology was observed in a Fe-0.5Cr-0.1C (wt. %) dual phase steel, whereas a globular austenite morphology was obtained in a Fe-4Cr-0.1C (wt. %) dual phase steel. Lenel *et al.* [1984] studied the formation of austenite from a starting microstructure consisting of ferrite and $M_{23}C_6$ carbides (coarse at grain boundaries and fine in the matrix). The nucleation of austenite is relatively sluggish, while the growth occurs rapidly (completed within 100 seconds at temperatures above Ae_3). The austenite inherits the Cr content of ferrite and no partitioning of Cr between ferrite and austenite accompanies the transformation.

Addition of alloying elements also affects the rate of formation of austenite; for example Judd *et al.* [1968], studied the effect of manganese on the formation of austenite. They found that Mn increases the incubation time for the nucleation and lower the nucleation rate of austenite. Although they explained the effect of Mn in terms of the carbide stability and diffusion fluxes in the system, but this seems to be somewhat speculative because manganese is an austenite stabilizer and should favour the formation of austenite.

2.6 An Assessment of the Kinetics of Reaustenitisation

2.6.1 Nucleation of Austenite

The kinetics of reaustenitisation are known to be a nucleation and growth process [Roberts and Mehl, 1943]. The nucleation site, growth rate and austenite morphology depend strongly upon on the initial microstructure of steels. Yi *et al.* [1985] studied the austenitisation process in an Fe-0.04C-2.20Si-1.8Mn (wt. %), and concluded that austenite is preferentially formed along the ferrite grain boundaries. Austenite formation along the grain boundaries proceeds rapidly, but its growth slows down after the site-saturation with austenite particles has occurred. The preferential sites for the nucleation of austenite are ferrite/ferrite grain boundaries in the case of the ferrite single phase starting microstructures [Speich and Szirmae, 1969], junctions of carbide particles and ferrite grain boundaries in the case of mixture of ferrite and carbide starting microstructures [Judd and Paxton, 1968; Lenel and Honeycombe, 1984a; Speich and Szirmae, 1969; Garcia and DeArdo, 1981] junctions between pearlite colonies and ferrite grain boundaries in the case of the mixture of pearlite and ferrite starting microstructures [Roberts and Mehl, 1943; Lenel and Honeycombe, 1984a; Speich and Demarest, 1981, Cai *et al.* 1985, Garcia and DeArdo, 1981] junctions between pearlite colonies in the case of pearlite

starting microstructures [Robert and Mehl, 1943; Speich and Demarest, 1981] prior austenite grain boundaries or martensite lath boundaries in the case of martensite starting microstructures [Baeyertz, 1942; Law and Edmonds, 1980; Matsuda and Okamura, 1974; Matsuda and Okamura, 1974] and prior grain boundaries in the case of bainite starting microstructures. In addition to these nucleation sites, carbide particles located at the boundaries between pearlite colonies and ferrite grains [Garcia and DeArdo, 1981], ferrite/ferrite boundaries and the retained austenite trapped between martensite laths [Yang and Bhadeshia, 1987; Yang, 1988; Yang and Bhadeshia, 1989; 14] have also been pointed out to play an important role for the nucleation of austenite.

2.6.2 The Growth of Austenite

The mechanism which governs the growth rate of austenite during reverse transformation from martensite, bainite and single phase ferrite has not been established. In the case of reaustenitisation from pearlite, the mixture of ferrite and pearlite, and the mixture of ferrite and spheroidised carbides, the growth of austenite is controlled by the diffusion of carbon in the austenite in the early stage of transformation [Speich and Demarest, 1981; Speich and Szirmae, 1969; Judd and Paxton, 1968; Lenel and Honeycombe, 1984a, 1984b; Hillert *et al.* 1971].

When the starting microstructure is pearlite, at high reaction temperatures, the partitioning of substitutional atoms becomes negligible because of the high supersaturation. In this case the diffusion of substitutional atoms is limited to an extremely short range although the long range diffusion of carbon atoms can occur with a diffusion distance about equal to the inter-lamellar spacing of the pearlite as discussed by Speich *et al.* [1981]. At low temperatures, in contrast, the long range diffusion of substitutional atoms might occur because of the low supersaturation, and the partitioning under local equilibrium at the interfaces will be achieved.

These two types of growth kinetics may appear at the first stage of the formation of austenite from the mixture of ferrite and pearlite until the dissolution of pearlite is complete.

After the completion of carbide dissolution in the mixture of ferrite and austenite, the situation might be same as that in the mixture of ferrite and carbides. In these cases, the kinetics governing the growth of austenite depend not only on the distribution of carbides [Hillert *et al.* 1971] or pearlite colonies but also on the reaction temperature. When carbides or pearlite colonies are distributed sparsely, interference between growing particles of austenite is negligible and the growth of

austenite in this situation will be controlled by carbon diffusion in austenite. For closely spaced carbides carbon diffusion in both austenite and in adjacent ferrite controls the growth of the austenite. At sufficiently low temperatures substitutional elements also diffuse during austenite growth.

In the case of the starting microstructure of martensite or bainite, the mechanism of the growth of austenite may be influenced by the carbides which have been formed during heat treatment or which exist in the initial microstructure. In these microstructures, the excess carbon exists either as carbides at ferrite grain boundaries or within the ferrite grains, or as solute in retained austenite or in martensite. The excess carbon trapped in the retained austenite or martensite may be exhausted by carbide precipitation during a heat treatment. The kinetics will then be the same as discussed in the case of the formation of austenite from the mixture of ferrite and carbides.

According to recent investigations [Yang and Bhadeshia, 1988, 1989, 1990; Yang, 1987] on reaustenitisation from a mixture of bainitic ferrite and residual austenite, the growth of austenite can satisfactorily be modelled in terms of one-dimensional carbon diffusion-controlled movement of the planar austenite-ferrite interfaces.

2.7 Summary

A survey of currently available literature on the formation of austenite has been presented. It can be concluded that both the nucleation and growth of austenite are largely dependent upon the initial microstructure, heating rate, and alloying elements. The preferred nucleation sites for the austenite are ferrite/ferrite grain boundaries or junctions of carbide and ferrite grain boundaries or prior austenite grain boundaries. The morphology of austenite also depends on the initial microstructure. If initial microstructure consists of ferrite laths for example bainite or martensite, the austenite adopts an acicular morphology otherwise grow in a globular morphology.



Chapter 3

EXPERIMENTAL: PROCEDURES AND TECHNIQUES

This chapter contains a brief description of the experimental alloys, heat treatments and other experimental procedures used in the research. Since the ultimate aim was to lay down the foundation for the modelling and prediction of the microstructures of high-strength steel weld deposits based on more rigorous theory, the microstructure as well as the behaviour under isothermal and continuous heating and cooling conditions, in order to establish the effects of parameters such as, alloy chemistry, cooling rate, *etc.*

3.1 Materials Selection

Since this study is mainly concerned with the Widmanstätten ferrite and bainite transformations, the selection of materials for this study was made, bearing in mind the following points:

- The materials should be of a high purity.
- The materials in some cases should have two separate C curves in the TTT diagram to avoid interference between Widmanstätten ferrite and bainite with the other transformations such as pearlite in the case of Widmanstätten ferrite and cementite precipitation in the case of bainite.
- The alloys should have at least two significantly different rates of transformation to cover all the morphologies of Widmanstätten ferrite and for the essence of the surface relief experiments.

It is already established that steels containing a large silicon concentration, bainite formation can occur without the precipitation of cementite [Bhadeshia and Edmonds, 1979, 1980, 1983]. Hence, high silicon alloys with different carbon concentrations were chosen. Because an aim of the present investigation is to improve the modelling of high strength steel weld deposits, some actual weld deposits were also studied. The chemical composition of all the alloys are given in Table 3.1. Alloys A1, A2, A3 and A4 ingots were hot rolled into round bars of 10 mm diameter. W1 was prepared by manual metal arc welding (MMA). The welding was carried out in the flat position using the stringer bead technique, the parent plate thickness being 20 mm. The welding current and voltage used were 180A and 23V (DC+) respectively (arc energy = 2 kJ mm⁻¹), the weld consisting of some 21 runs with 3 runs per layer deposited at a speed about 0.002 ms⁻¹, the electrode diameter was 4 mm. These weld deposits were provided by ESAB (UK) Ltd.

Table 3.1: *Chemical composition of the materials used in present study.*

Alloy design.	Chemical Composition												
	(wt%)										(ppm)		
	C	Si	Mn	Cr	Mo	Ni	Cu	Nb	V	Ti	Al	O	N
A1	0.220	2.07	3.00	-	0.00	-	-	-	-	-	-	6	-
A2	0.220	2.05	3.07	-	0.70	-	-	-	-	0.004	0.005	94	-
A3	0.120	0.30	0.50	2.50	1.00	-	-	-	-	-	-	-	-
A4	0.400	2.00	-	-	-	-	-	-	-	-	-	-	-
A101	0.059	1.96	2.88	-	-	-	-	-	-	-	-	-	-
A102	0.120	2.03	2.96	-	-	-	-	-	-	0.004	0.005	14	-
A103	0.059	1.94	-	-	-	4.07	-	-	-	0.004	0.009	1900	-
A104	0.096	2.00	-	-	-	4.07	-	-	-	-	-	-	-
W-1	0.067	0.44	1.22	0.50	0.01	0.64	0.39	0.01	0.02	-	-	350	91

3.2 Specimen Preparation

Two types of specimens were used; 10 mm long rods of 3 mm diameter were used for isothermal heat treatments and optical microscopy. The 3 mm diameter was selected to facilitate transmission electron microscopy at any stage of the experiments. Whereas 10 mm square rods were used, for surface relief experiments.

The 3 mm diameter rods were produced by swagging, involving a successive reduction in the diameter in approximately 1 mm steps. It was necessary to initially hot swagged down to 6 mm diameter rod. After removing 2 mm from the surface, these were further swagged down to 3 mm rods at ambient temperature in order to avoid oxidation.

3.3 Heat Treatment Procedures

The heat treatment cycles are illustrated Fig. 3.1 and are described below:

3.3.1 Homogenisation

After swagging, the 3 mm diameter rods were homogenized at 1250 °C for 3 days while sealed in quartz tubes containing a partial pressure of high purity

argon. The homogenisation treatment was carried out in a resistance-heated horizontal tube furnace and the temperature was measured with a Pt-Pt 13 wt% Rh thermocouple. The temperature was controlled within the limits of ± 5 °C.

3.3.2 Austenitisation

Before any isothermal transformation austenitisation treatments generally performed at 1100 °C for 10 min to produce larger austenite grains, while the specimens were sealed in quartz capsules under a partial pressure of pure argon.

3.3.3 Isothermal Transformation

After austenitisation the samples were taken out from the furnace, the quartz capsule was carefully broken and then immediately quenched into a fluidized bed, which was maintained at the reaction temperature (controlled to ± 3 °C), for specified duration and then finally quenched into iced-water.

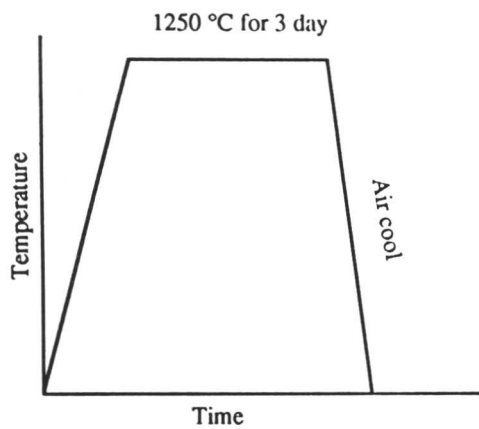
It was felt essential to break the silica capsules before the commencement of isothermal transformation, to bring the specimen concerned to the transformation temperature as quickly as possible.

The powder in the bed was fluidized by introducing air through the bottom of the bed. The flow rate of the air in the outer chamber was maintained at $250 \text{ cm}^3 \text{ min}^{-1}$, while in the inner chamber it was $84 \text{ cm}^3 \text{ min}^{-1}$. A uniform temperature was maintained in the fluidized bed under these flow conditions.

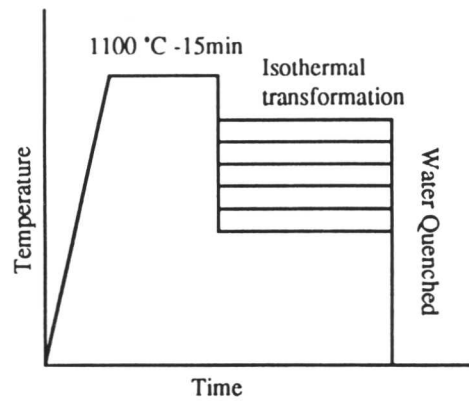
3.4 Surface Relief Experiments

For surface relief experiments, specimens were mechanically polished to a $1/4 \mu\text{m}$ finish, and sealed in quartz capsules. Before sealing, the capsules were flushed several times with high purity argon gas to minimize oxidation at the mirror-surface of the specimen. The capsules were finally sealed off with a partial pressure of argon. The heat treatments were carried out in the same way as described in the previous section except that after austenitisation, the quartz capsules were not broken but simply transferred to the fluidized bed maintained at the reaction temperature, reacted for the predetermined time and then quenched into ice cooled water.

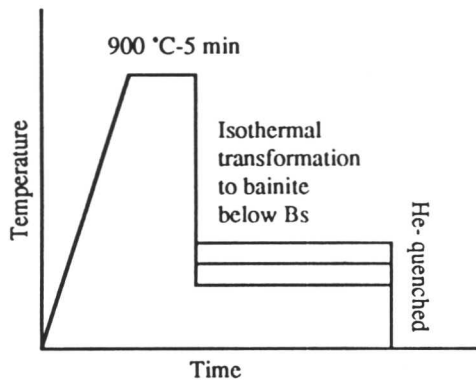
Any surface relief effects were imaged using the Nomarski differential interference technique with a Ziess optical microscope. The tilt sense was determined by through focusing experiments, using grain boundary grooves for reference. Upward upheavals consisting of two adjacent and opposing invariant-plane strains are referred to as “tent-like” compared with a similar net depression of the free surface which are referred to as “vee-shaped” surface relief effects.



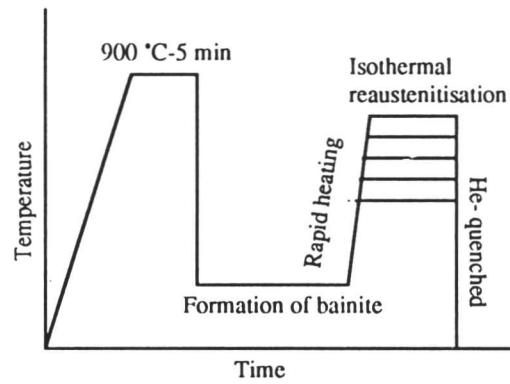
a) For homogenisation after swaging.



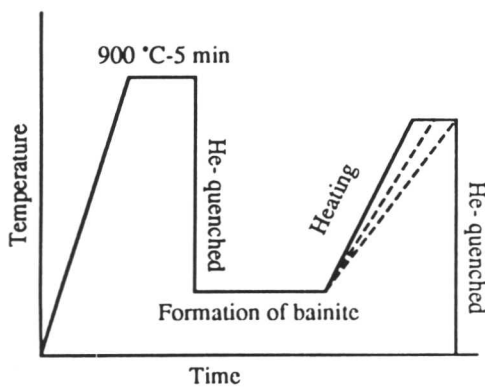
b) For isothermal transformation to Widmanstätten ferrite.



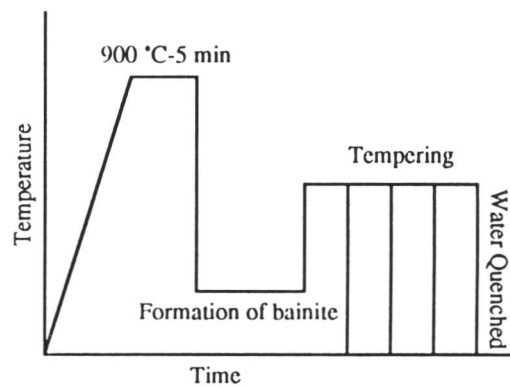
c) For bainite transformation.



d) For isothermal reaustenitisation from bainite microstructure.

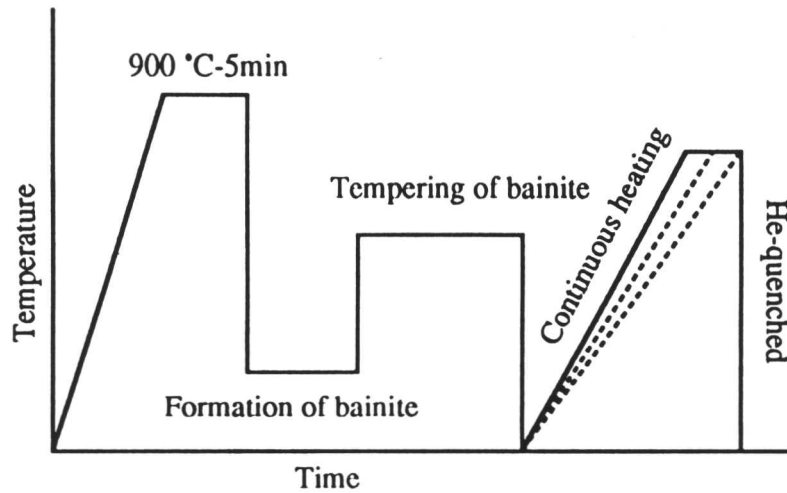


e) For Continuous heating from bainite microstructure.

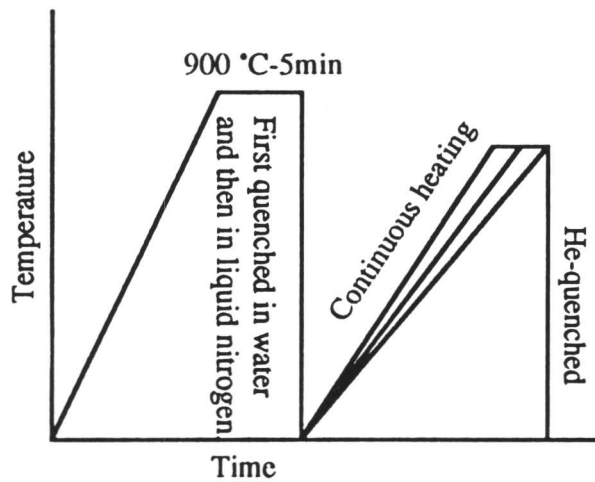


f) For Tempering of bainite.

Fig. 3.1: Continued.....



g) For re-austenitisation from tempered bainite.



h) For re-austenitisation from martensite microstructure.

Fig. 3.1: Schematic illustrations of the heat treatments cycles used in the present study.



Fig. 3.2: Photograph showing the dilatometer and its test chamber, as used in this study.

3.5 Dilatometry

Dilatometry is a powerful technique to study the kinetics of phase transformation. All dilatometry was performed on a Theta Industries high speed dilatometer (shown in Fig. 3.2), which has a water cooled radio-frequency furnace of essentially zero thermal mass, since it is only the specimen which undergoes the programmed thermal cycle. The length transducer on the dilatometer was calibrated using a pure platinum specimen of known thermal expansion characteristics. The dilatometer has been specially interfaced with a BBC/Acorn microcomputer so that length, time and temperature information can be recorded at microsecond intervals during the heat cycle, and the data are stored on a floppy disc. The information is then transferred to a mainframe IBM3084 computer for further analysis.

3.5.1 Specimens for Dilatometry

Two types of specimen were used, solid cylindrical (SC) and hollow thin walled cylindrical (HTWC) as shown in Fig. 3.3, depending upon the transformation kinetics of the material. SC specimens for dilatometry were machined in the form of 3 mm diameter rods with about 20 mm of length. To obtain higher heating or cooling rates HTWC specimens were machined in the form of 4 mm diameter rods

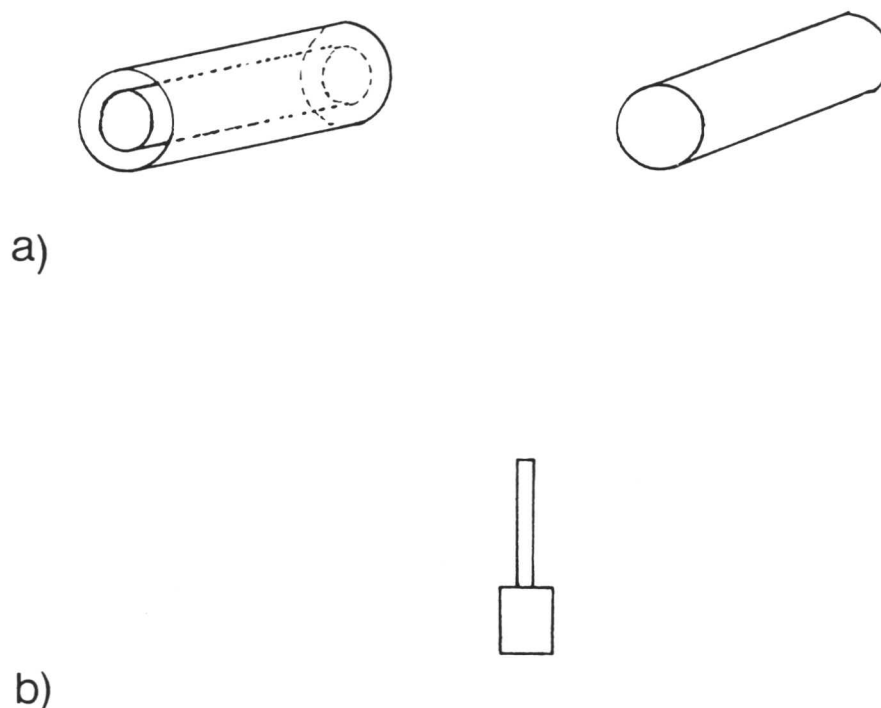


Fig. 3.3: Schematic diagram of the specimens used; a) for dilatometry and b) for lattice parameter measurements.

with 2.5 mm bore through it, to get a reduced wall thickness with about 10 mm of length.

3.5.2 Nickel Plating

To avoid surface nucleation and surface degradation, all dilatometry specimens were plated with nickel. This nickel plating process is in two stages; nickel striking and nickel plating. Striking was carried out in a solution made up of 250 g nickel sulphate, 27 ml concentrated sulphuric acid and distilled water, amounting to one litre in all, at 50 °C with a current density of 7.75 mA/mm² for three minutes. The plating solution consisted of 140 g nickel sulphate, 140 g anhydrous sodium sulphate, 15 g ammonium chloride and 20 g boric acid, was made up to one litre with distilled water. The plating was carried out at 50 °C with a current density of 0.4 mA/mm² for fifteen minutes. This two process finally give a plate thickness of approximately 0.08 mm.

3.6 Metallography

For optical metallography the heat treated specimens were hot mounted in an acrylic plastic, and ground on silicon carbide paper in continuous flow of water. Care was taken during initial grinding to remove sufficient material to avoid any unrepresentative surface caused by decarburization during heat treatment. They were then mechanically ground to 1200 grade emery paper and finally polished with 6, 1, and 1/4 μm diamond pastes respectively.

After final polishing, the specimens were thoroughly cleaned and washed in methanol. Optical specimens were etched in 2 Nital solution (2 ml of HNO₃ in 100 ml of methyl alcohol) and were examined using an OLYMPUS microscope, fitted with a 35 mm camera.

3.7 Transmission Electron Microscopy

Thin foil specimens were prepared for transmission electron microscopy from 0.25 mm thick discs slit from heat treated specimens used in the dilatometry. The discs were thinned to about 0.04 mm by abrasion on 1200 grade emery paper and then electro-polished in a twin jet electro-polisher using a 5% perchloric acid, 25% glycerol and 70% ethanol mixture solution at ambient temperature, at about 50 V. The microscopy was conducted on a PHILIPS EM400 transmission electron microscope operated at 120 kV.

3.8 Extraction Replicas

The extraction replica technique is very useful for the study of carbide or precipitate phases in a metallic system. The main advantages of replicas over foils are that they eliminate any effects due to the steel matrix and thus enable the chemical composition of the carbides to be measured more accurately, and working with a magnetic specimen in the electron microscope is avoided. The replica is also very thin $\simeq 100\text{\AA}$, has no self-structure and will not burn in an electron beam.

Carbon extraction replicas were prepared using the method described by Smith and Nutting [1956]. Firstly, the metal surface was prepared using the same method and etchant as for optical microscopy, and then a bluish-brown layer of amorphous carbon was deposited onto the metal surface using a vacuum evaporator. The film was then scored using a sharp blade to enable removal of several small sections covering the whole area of the sample, and then electrolytically etched in a solution of 5% chloral (hydrochloric acid in methanol) at +1.5V until the edges of the film began to lift away from the surface. The specimen was washed in ethanol, and then in distilled water in which the replicas floated off and were collected on copper grids. The replicas were then examined in the TEM usually using an accelerating voltage of 120kV.

3.9 Microanalysis

All microanalysis carried out on EM 400T transmission electron microscope fitted with a LINK 860 energy dispersive analysis system. Standard thin foil correction programmes were used to compensate for X-ray detection efficiency and absorption. For quantitative analysis the specimen was tilted by 35° towards the detector in order to optimise the signal.

3.10 Measurement of Lattice Parameter

The detailed analysis of dilatometric data requires a knowledge of ferrite lattice parameter, since the addition of various alloying elements to pure iron not only effects their mechanical properties but also the lattice parameter of the crystals.

3.10.1 *Materials and Specimen Preparation*

The lattice parameters of five different steels were measured, and the steels can be categorized into two groups i.e., Fe-C-Si-Mn steels and Fe-C-Si-Ni steels (Table 3.1)

Two types of specimens 0.5 ± 0.01 mm wire and fillings were used (Fig. 3.3). Before preparation from bulk material, samples were annealed at 600°C for 2 hr,

while sealed in silica capsules under a partial pressure of argon, in order to induce the thermal decomposition of any retained austenite.

The specimens were then machined from the annealed 3.0 mm diameter rods. After machining, specimens were chemically polished in a solution containing 5 % HF, 45 % H₂ O₂ and 50 % H₂ O in order to remove the surface by about 0.1 mm to relieve any stresses induced during the machining operation.

Filings were obtained from annealed specimens, and were then re-annealed in silica capsules containing pure argon atmosphere, at 600 °C for 1 hr and finally cooled in the furnace to room temperature.

Lattice parameter measurements were carried out using a Debye-Scherrer camera. In order to get sufficient number of reflections, zirconium filtered molybdenum K α radiation was used.

3.11 Hardness Testing

Macro hardness were measured with Vicker's hardness testing machine using 10 kg load. While micro hardness measurements have been carried out on a Leitz hardness measuring machine. This instrument equipped with a digital eyepiece to which a computer-counter-printer was attached. Specimens were polished and etched by 2% Nital before the measurement of micro hardness. The indentation load applied was either 0.0981 N or 98.1 N.



Chapter 4

STUDY OF THE BAINITE TRANSFORMATION USING DILATOMETRY

4.1 General Introduction and Scope

Classical bainite is a non-lamellar mixture of ferrite and carbide [Davenport *et al.* 1930; Mehl, 1939], generally regarded as an aggregate of ferrite and *residual phases*, such as retained austenite, carbide or martensite. The bainite transformation is of particular importance to industry, because steels in the bainitic condition can show a very good combination of strength and toughness [Nakasugi *et al.* 1983]. It exhibits various features which are different from *reconstructive*§ transformations such as allotriomorphic ferrite and idiomorphic ferrite or even those which also form by a *displacive*§ transformation mechanism *e.g.*, Widmanstätten ferrite, in which only the interstitials diffuse. Bainite nucleates with an equilibrium carbon content but grows without diffusion [Bhadeshia, 1981a]. It consequently stops growing when the carbon concentration of austenite reaches a value given by the T_0 curve of the parent alloy. While Widmanstätten ferrite nucleates by the same mechanism, it grows by an equilibrium or paraequilibrium mechanism and does not show an *incomplete reaction phenomenon*§.

Dilatometry is an important tool for the study of phase transformations in steels and widely used in industry because of its sensitivity and accuracy. This technique, has in the past been applied to the study of the bainite transformations, but during without sufficient interpretation of the data, it has often been incorrectly assumed that the transformation can proceed to a point where all the austenite is consumed. This interpretation of experimental data has apparently misled several researchers [Ohmori *et al.* 1971; Umemoto *et al.* 1982].

§ Reconstructive transformations are those which form as result of lattice reconstruction process by diffusion [Bhadeshia, 1987].

§ Displacive transformations are those which form without the reconstruction of lattice, atoms just displace in a manner that they can maintain correspondence between product and parent phase, these products show various features which are similar to martensitic transformation [Bhadeshia, 1987].

§ At any temperature (below B_G), and in the absence of any interfering secondary reactions, only a limited quantity of bainite forms before the reaction terminates, which is far less than that expected by the Lever rule at that temperature. This premature termination of the bainite transformation is known as “incomplete reaction phenomenon”.

This work is aimed at the further exploration of aspects of bainite transformation in high-strength steels in the context of recent studies [Bhadeshia, 1982]. Steels containing about 2 wt.% silicon as an alloying element were used; these steels can be isothermally transformed to just bainitic-ferrite and residual austenite [Bhadeshia *et al.* 1979, 1983], the formation of carbides being completely suppressed. Hence, the kinetic measurements relate directly to the displacive formation of bainitic-ferrite, without interference from any of the additional, diffusional reactions (such as precipitation of carbides) which accompany the formation of bainite in conventional steels.

4.2 Experimental Techniques

For the present study, those materials were selected in which bainite transformation can be studied without the interference of other transformations such as pearlite and precipitation of carbides. The chemical composition of the steels used are listed in Chapter 3, but are reiterated here for convenience (Table 4.1). The other details (such as microscopy) have been discussed fully in Chapter 3.

Table 4.1: *Chemical composition of the steels used in the present study.*

Steel	Chemical Composition (wt. %)							
	C	Si	Mn	Ni	Mo	Ti	Al	O (ppm)
A2	0.22	2.05	3.07	–	0.7	0.004	0.005	94
A101	0.059	1.96	2.88	–	–	–	–	–
A102	0.12	2.03	2.96	–	–	0.004	0.005	14
A103	0.096	2.0	–	4.07	–	0.004	0.009	1900
A104	0.05	1.94	–	4.04	–	–	–	–

4.2.1 Lattice Parameter of Ferrite

To study phase transformations in steels using dilatometry, it is essential to have a knowledge of the lattice parameter of ferrite, since the addition of various alloying elements to pure iron not only effects their mechanical properties but also the lattice parameter of the crystals. Work was undertaken to measure the lattice parameter of ferrite for five of the steels used in the present studies.

Lattice parameter measurements were carried out using a Debye-Scherrer camera. In order to get a sufficient number of reflections, zirconium filtered molybdenum $K\alpha$ radiation was used.

4.3 Results and Discussion

Using the films obtained using the Debye-Scherrer analysis, the distances between the θ values (Bragg angles) were measured with a travelling microscope, and a pairs of vernier callipers. Each film was measured at least three times and mean values were taken for subsequent calculations as shown in Table 4.2.

From these data, the d spacings of the planes were obtained via the Bragg law and analysed by plotting $d\sin^2\theta$ or the Nelson-Riley function; both of these functions are based on the fact that errors are minimised at large values of θ [Cullity, 1978]. This is because the angular position of the diffracted beam is much more sensitive to a given change in plane spacing when θ is large than when it is small. Nelson and Riley [1945] and Taylor and Sinclair [1945] analysed the various sources of error, particularly absorption, which can be significant for steel specimens of the two functions, the relation suggested by Nelson and Riley holds quite accurately down to low values of θ , so that calculate lattice parameter values were extrapolated against $(\frac{\cos^2\theta}{\sin\theta} + \frac{\cos^2\theta}{\theta})$ rather than $\sin^2\theta$. The results are shown in Fig. 4.1, and the measured values of lattice parameter (a) are given in Table 4.2.

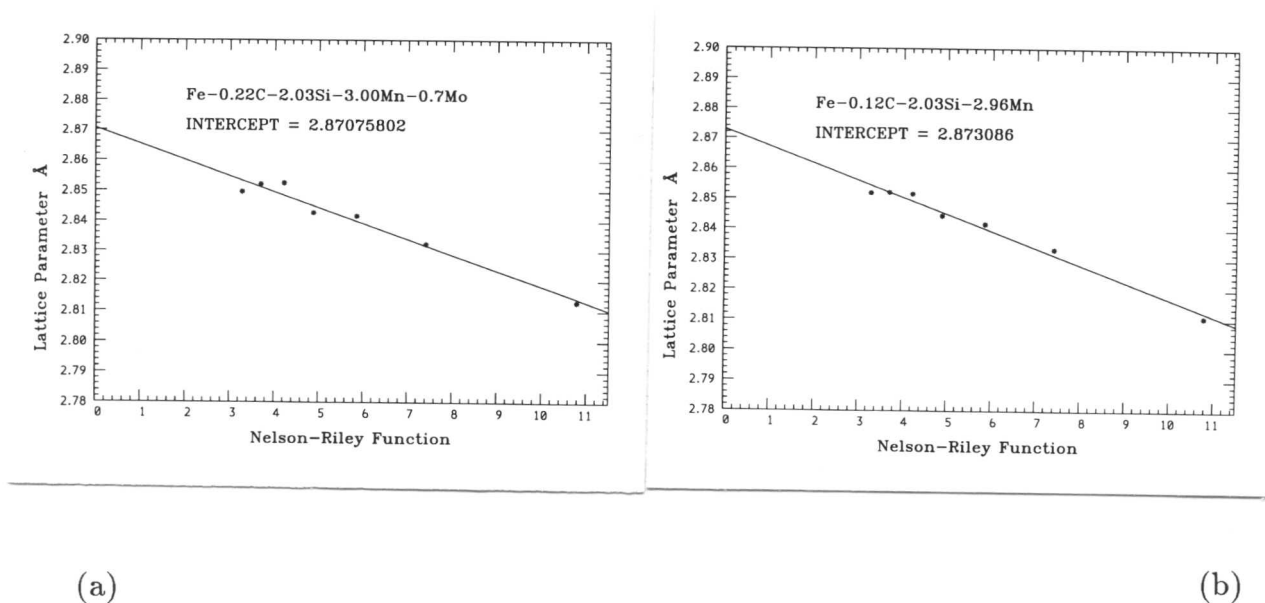
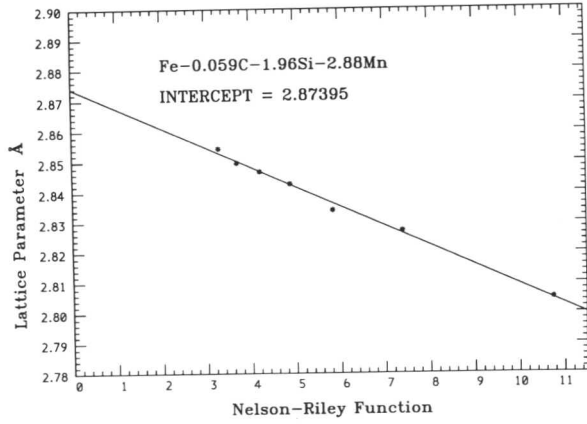
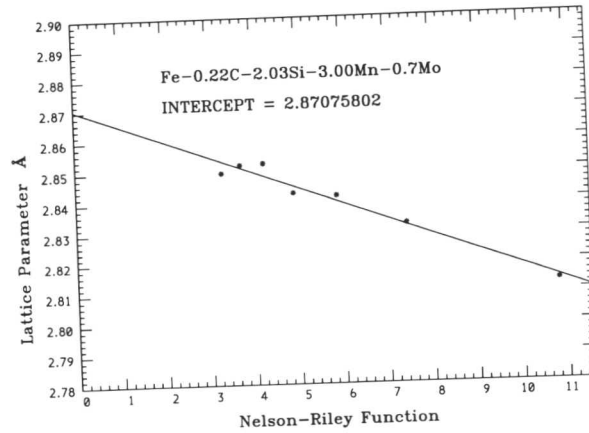


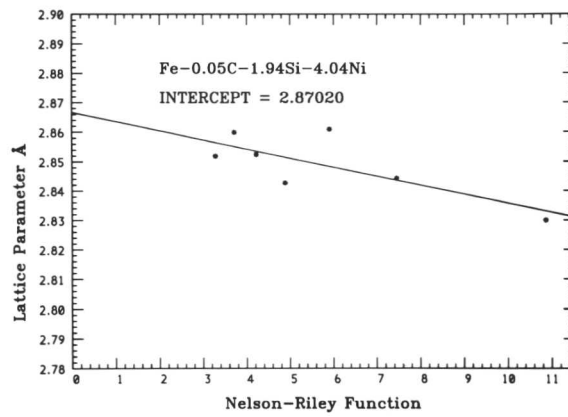
Fig. 4.1: *Continued.....*



(c)



(d)



(e)

Fig. 4.1: Extrapolation of measured d -spacings against Nelson-Riley function [1947], for alloys (a) A2, (b) A101, (c) A102, (d) A103, and (e) A104.

Table 4.2: *Measured lattice parameters of the steels used.*

Steel	Measured Lattice Parameter (Å)
A2	2.8670 ± 0.001
A101	2.8739 ± 0.003
A102	2.8730 ± 0.002
A103	2.8722 ± 0.001
A104	2.8702 ± 0.001

4.4 Expansivities of Ferrite and Austenite

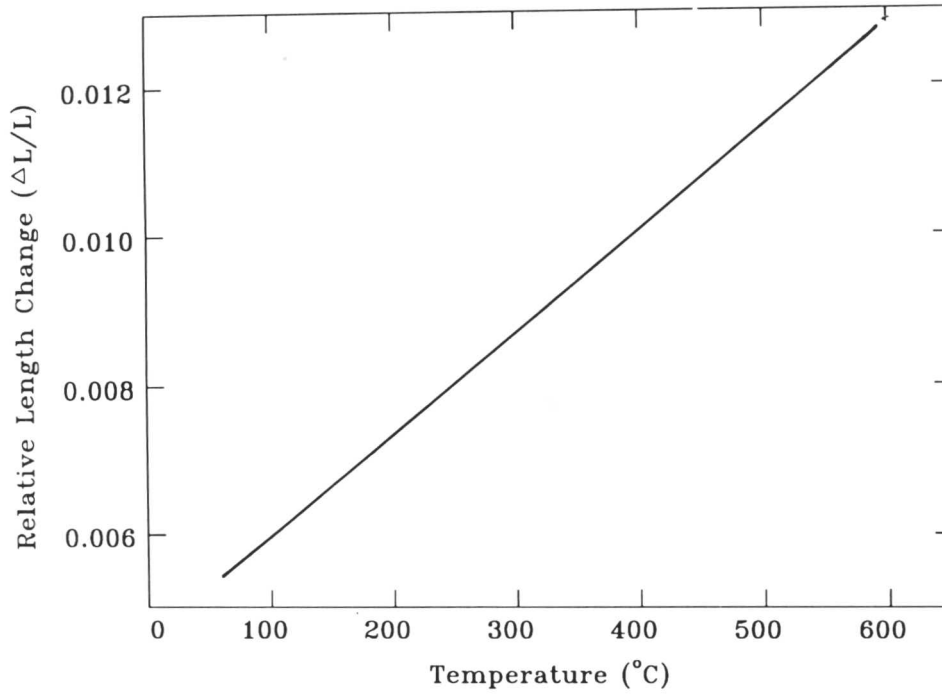
The interpretation of dilatometer data also requires a knowledge of the expansion coefficients of ferrite (e_α) and austenite (e_γ). The ferrite expansion coefficient was determined by first tempering a specimen at 600 °C for 10 min to decompose any retained austenite and then recording the length change during heating and cooling at rate of 0.001 °C s⁻¹. The measurements do not therefore account for the presence of a small amount of carbide phase. The graphs of relative length versus temperature are plotted in Fig. 4.2. The expansion coefficient of austenite was measured while the specimen was in the γ single-phase field (Table 4.3).

Table 4.3: *Measured expansion coefficient of ferrite and austenite.*

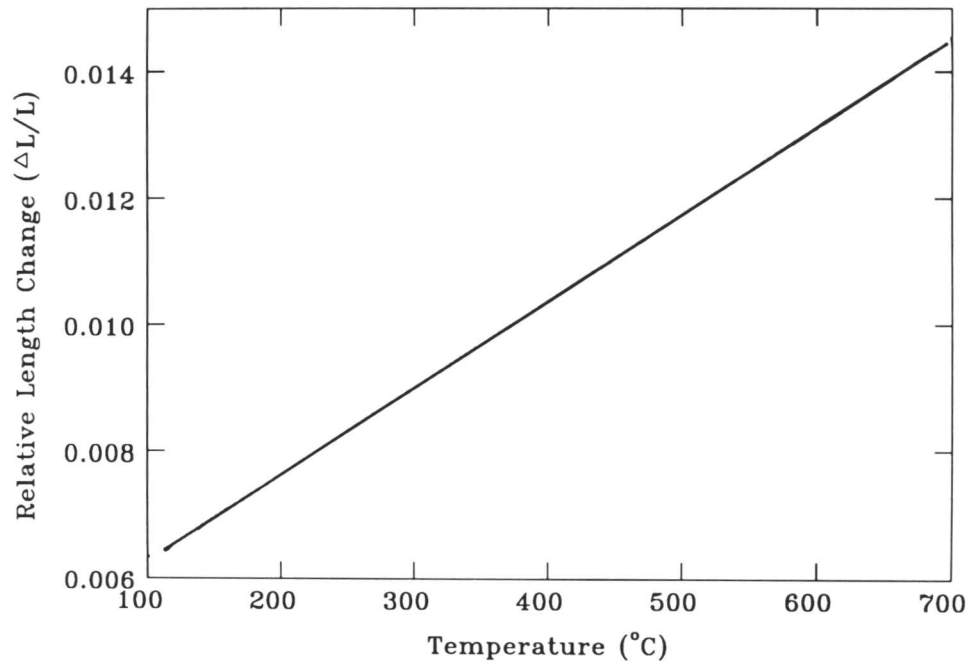
Steel	Expansion Coefficient (°C ⁻¹)	
	Ferrite	Austenite
A2	$1.443 \times 10^{-5} \pm 0.004$	$2.205 \times 10^{-5} \pm 0.027$
A101	$1.416 \times 10^{-5} \pm 0.044$	$2.010 \times 10^{-5} \pm 0.064$
A102	$1.435 \times 10^{-5} \pm 0.002$	$2.0756 \times 10^{-5} \pm 0.010$
A104	$1.401 \times 10^{-5} \pm 0.021$	$2.021 \times 10^{-5} \pm 0.020$

4.5 Theory for the Conversion of Dilatometry Data

For the transformation of austenite (γ) into a mixture of bainitic ferrite and carbon-enriched austenite, Bhadeshia [1982] has shown that the relative length change $\frac{\Delta L}{L}$, which is the observed length change divided by the length of the specimen, can be related to the volume fraction of ferrite (V_α) by the equation:

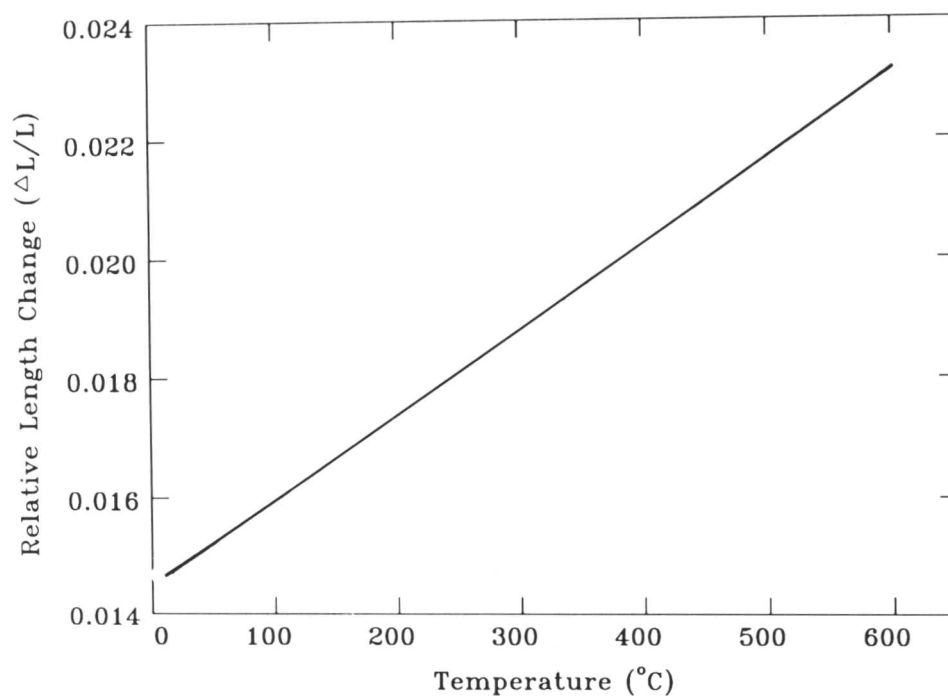


(a)

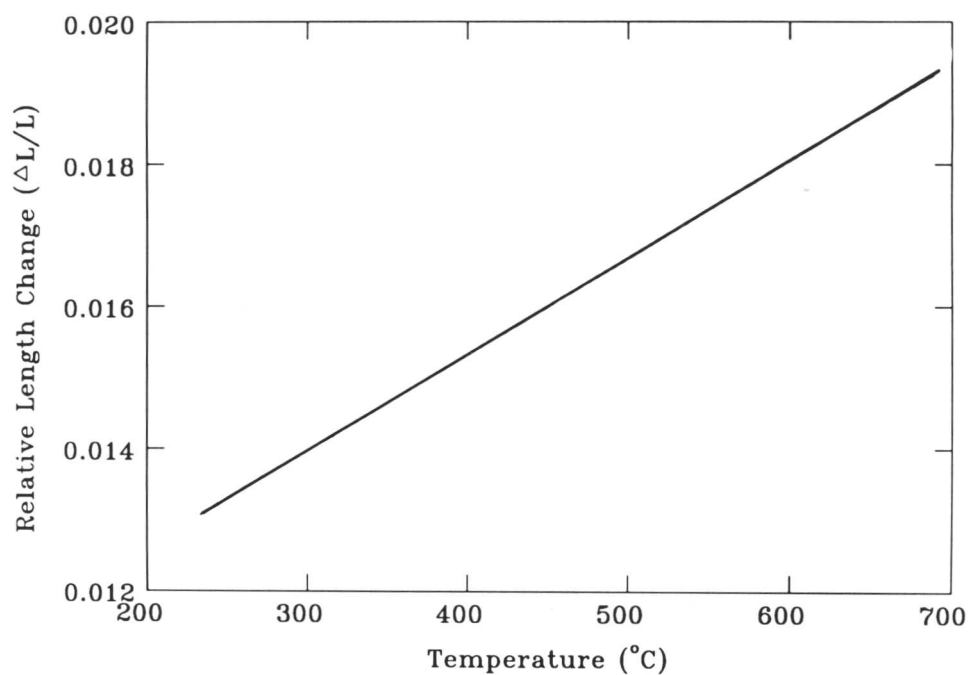


(b)

Fig. 4.2: *Continued*



(c)



(d)

Fig. 4.2: Showing the graph of relative length change versus temperature, from which the linear expansion coefficient of ferrite was obtained in alloy (a) A2, (b) A101, (c) A102, (d) A104.

$$\frac{\Delta L}{L} = \frac{2V_\alpha(a_\alpha^3) + (1 - V_\alpha)(a_\gamma^3) - a_{\gamma_0}^3}{3a_{\gamma_0}^3} \quad (4.1)$$

with

$$a_\alpha = a_{\alpha_0}(1 + e_\alpha(T - 25))$$

$$a_{\gamma_0} = (C_1 + C_2\bar{x} + C_{Si}x_{Si} + C_{Mn}x_{Mn} + C_{Mo}x_{Mo})(1 + e_\gamma(T - 25))$$

$$a_\gamma = (C_1 + C_2\bar{x} + C_{Si}x_{Si} + C_{Mn}x_{Mn} + C_{Mo}x_{Mo})(1 + e_\gamma(T - 25))$$

The Coefficients C_i have been determined by Dyson *et al.* [1970]; x_i represent the concentrations of alloying additions.

The carbon content of residual austenite x_γ is related to the volume fraction V_α of ferrite is expressed by

$$x_\gamma = \frac{\bar{x} - V_\alpha S}{1 - V_\alpha} \quad (4.2)$$

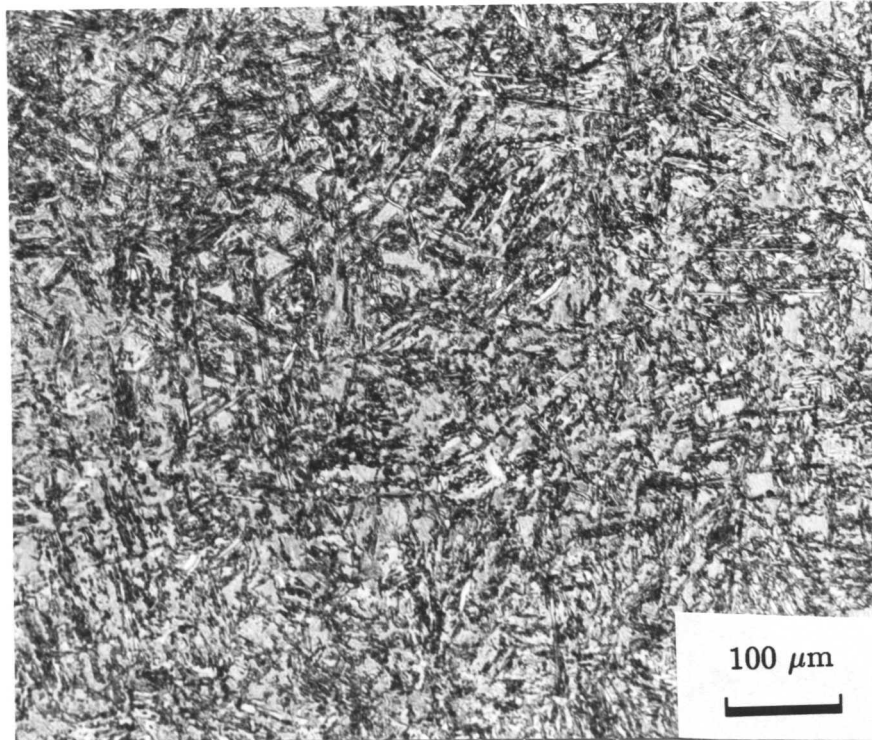
where \bar{x} and S are the average carbon concentration of the steel and carbon content of ferrite respectively. Equation (4.1) can be solved iteratively to give x_γ from $\frac{\Delta L}{L}$ measurements.

4.6 Bainite Transformation

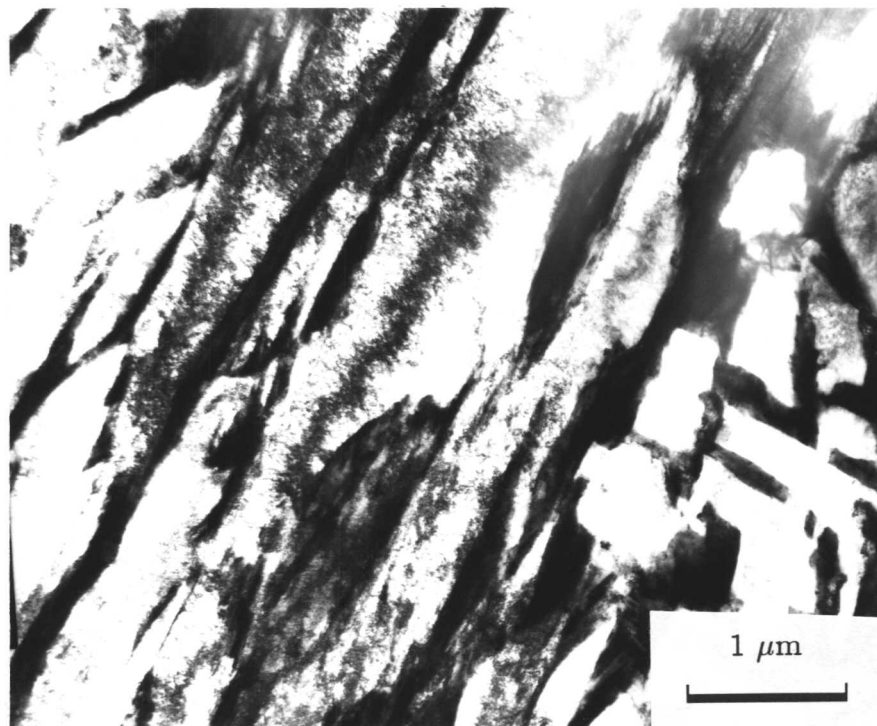
Fig. 4.3 shows the bainitic microstructure in a Fe-C-Si-Mn alloy consisting of classical sheaves of bainite nucleating at prior austenite boundaries. Transmission electron microscopy revealed (as expected) that the sheaves were composed of much smaller sub-units of ferrite and the microstructure did not contain any carbide precipitation. Only bainitic ferrite and carbon-enriched austenite could be seen; the bainite reaction did not go to completion despite prolong periods of holding at isothermal transformation.

It was found that near the B_S temperature only very limited amount of austenite transformed to bainite but as the isothermal transformation temperature decreased, correspondingly larger quantities of bainite were observed (Fig. 4.4). It is clear that in the specimen transformed above the calculated B_S temperature (Table 4.4) *i.e.*, at 520 °C, there is very little bainite, while in the specimens transformed at 500 °C and 480 °C, a large degree of transformation can be observed.

The dilatometry results (Figs. 4.5 and 4.6) also showed the relative length change during the formation of bainite increases as the isothermal transformation temperature decreases below the B_S temperature. The amount of bainite formed is dependent on the transformation temperature below B_S , consisted with the optical microscopy.



(a)



(b)

Fig. 4.3: Micrographs showing bainite microstructure in alloy A2. (a) Optical micrograph. (b) TEM micrograph. Specimen isothermally transformed at 400 °C for 1000 s after austenitisation at 900 °C for 5 min.

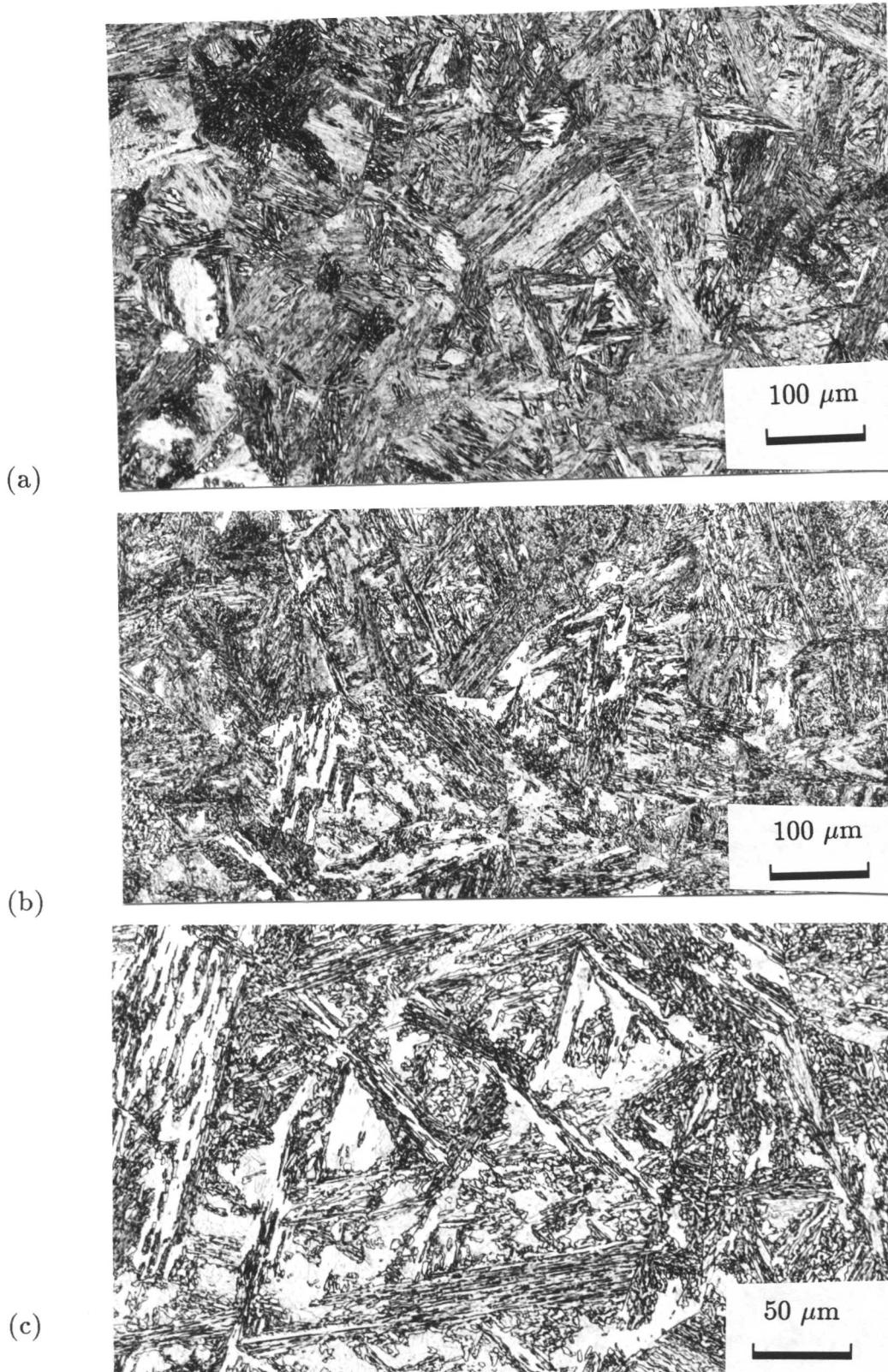


Fig. 4.4: *Optical micrographs showing the effect of isothermal transformation temperature on bainite formation in alloy A102. Specimens austenitised at 1300 °C for 10 min and isothermally transformed for 200 s at (a) 560 °C (b) 520 °C (c) 480 °C. Note that the amount of bainite increases as the isothermal transformation temperature decreases.*

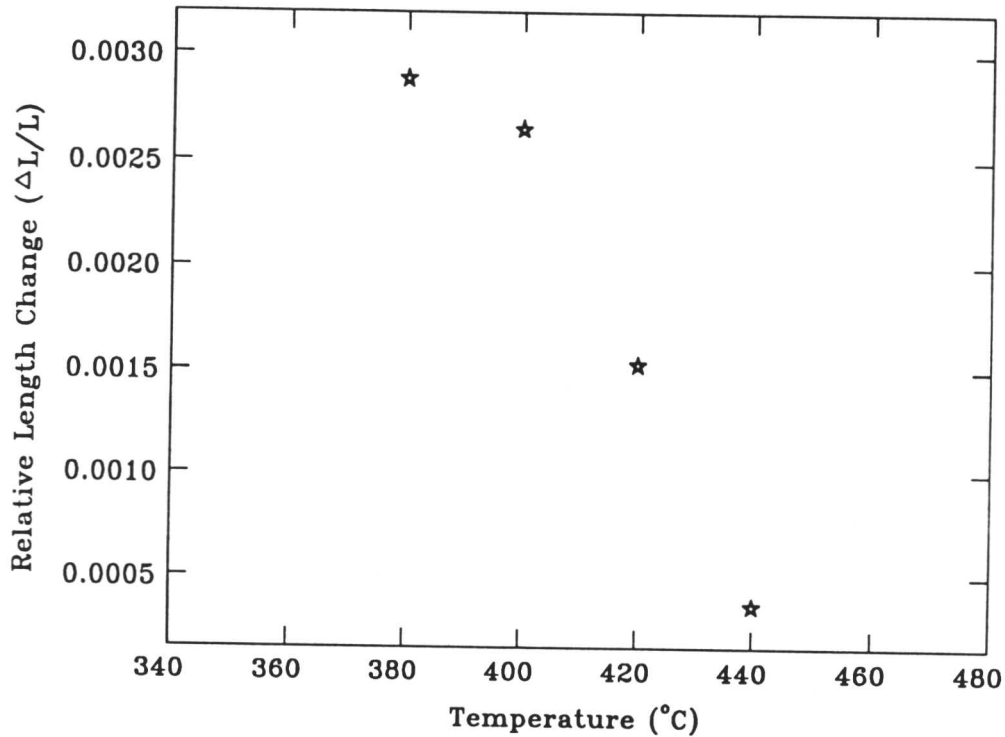


Fig. 4.5: Effect of isothermal temperature on the maximum relative length change observed by dilatometry in alloy A2.

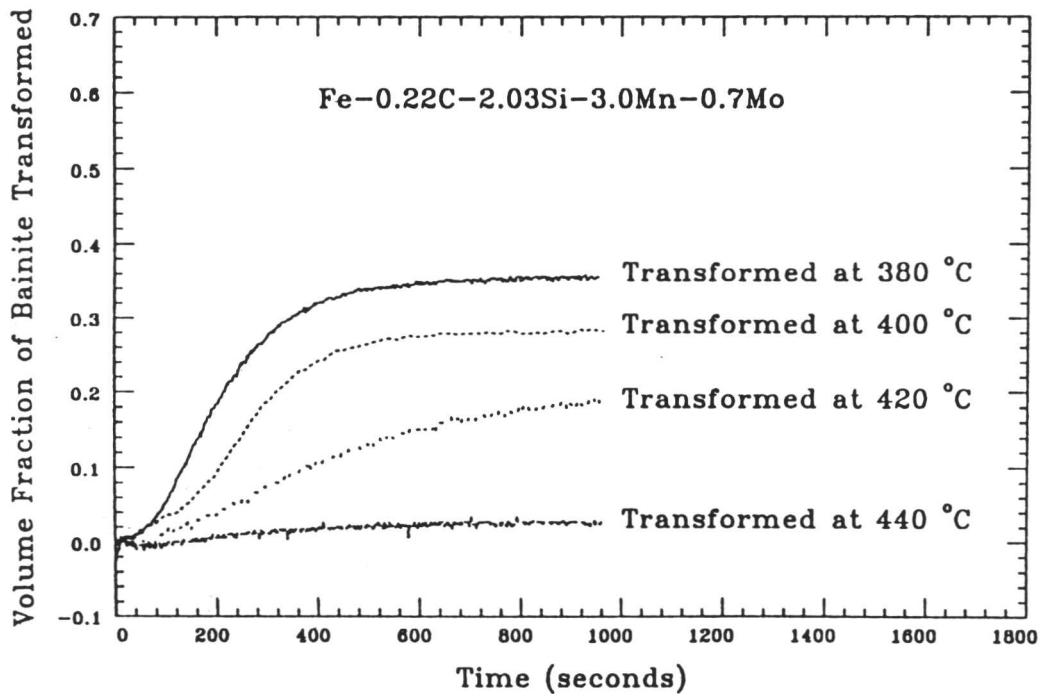


Fig. 4.6: Effect of isothermal temperature on the formation of bainite below B_S temperature in alloy A2. Note that the maximum extent of bainite transformation is increases with an decrease in isothermal transformation temperature.

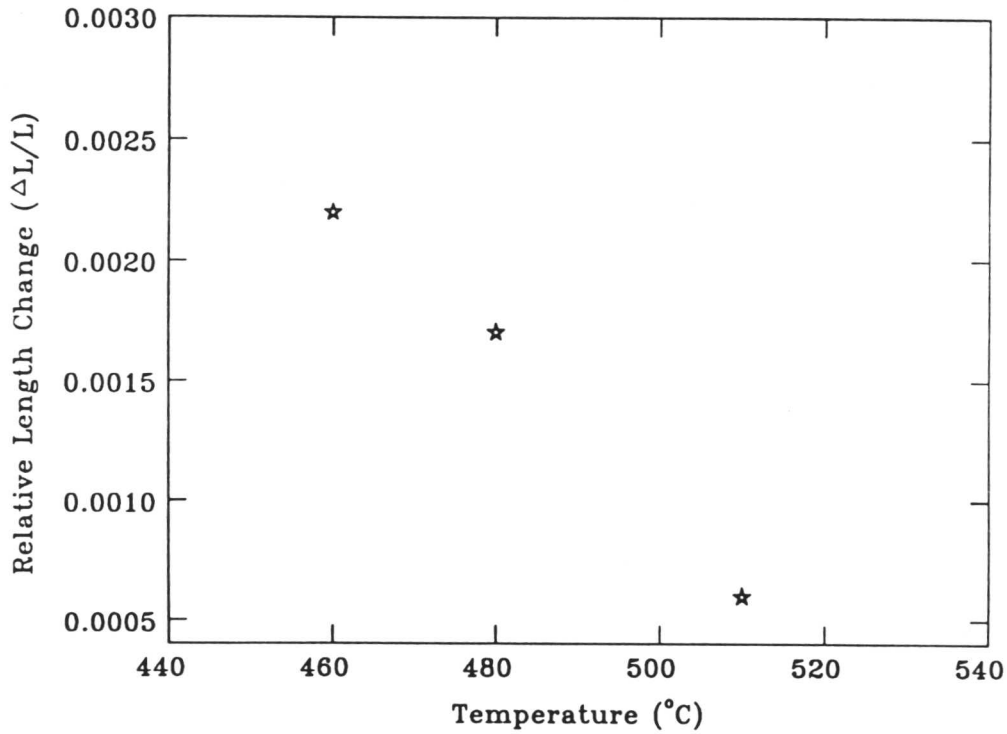


Fig. 4.7: Effect of isothermal temperature on the maximum relative length change observed by dilatometry in alloy A102.

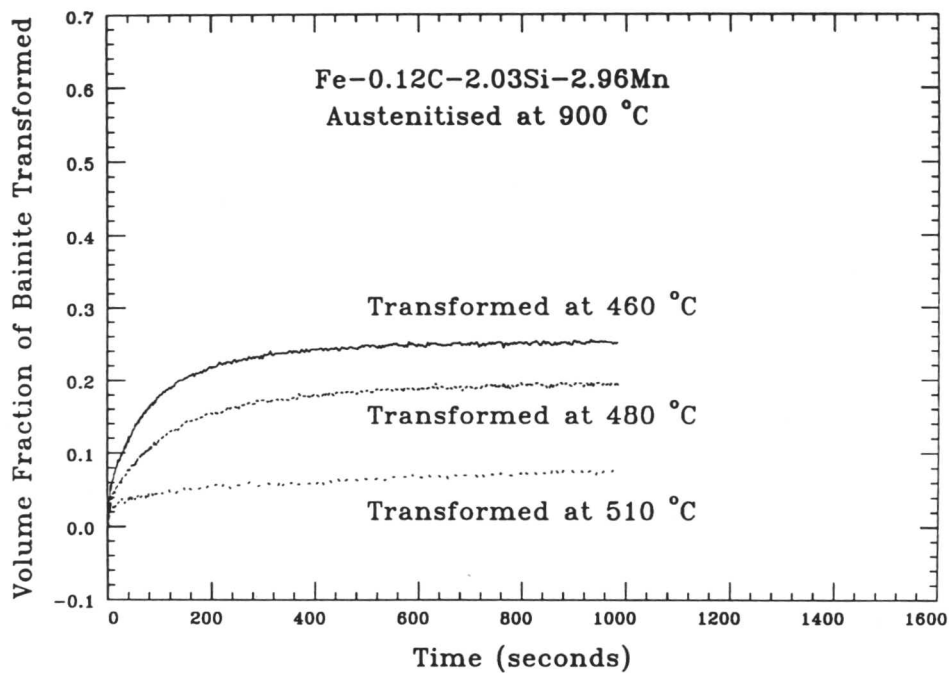


Fig. 4.8: Effect of isothermal temperature on the formation of bainite below the B_S temperature in alloy A102. Note that the maximum extent of bainite transformation increases with a decrease in isothermal transformation temperature.

The reaction proceeds initially rapidly but after a period the decomposition slows down as is shown in Figs. 4.7 and 4.8.

Table 4.4: *Calculated transformation-start temperatures for the steels studied (calculated by using the methods discussed by Bhadeshia and Edmonds, 1979; Bhadeshia, 1981c; 1981d.)*

Alloy No.	Ae_3	Ae'_3	W_S	B_S	M_S
A2	812	773	700	477	338
A101	864	828	760	545	422
A102	812	776	745	520	390
A103	800	774	680	552	444
A104	812	784	680	564	460

In alloys A101 and A104, the bainite occurred very rapidly with some transformation happening during cooling to the transformation temperatures. It follows that the relative length change measured at the intended temperature T_i , should be corrected as follows [Yang and Bhadeshia, 1987] as shown in Fig. 4.9. In the absence of transformation during cooling to the isothermal transformation temperature, the length of the specimen will vary linearly with temperature as the sample contracts. Any deviation from linearity indicates transformation during cooling. If the lower temperature part of the curve is extrapolated to the reaction temperature, the vertical difference between the extrapolated line and the actual length change curve gives the true length change due to transformation, as if no reaction had occurred during cooling. The maximum corrected relative length change is then ΔL_f instead of L_i as illustrated in the Fig. 4.9. It is necessary to remove the effect of the transformation during cooling to T_i , the length increment associated with cooling from T_s to T_i ;

$$\Delta L_f = L_i \{1 + e_\alpha(T_s - T_i)\} \quad (4.3)$$

The corrected relative length change for the data shown in Table 4.5 and are plotted in Fig. 4.10.

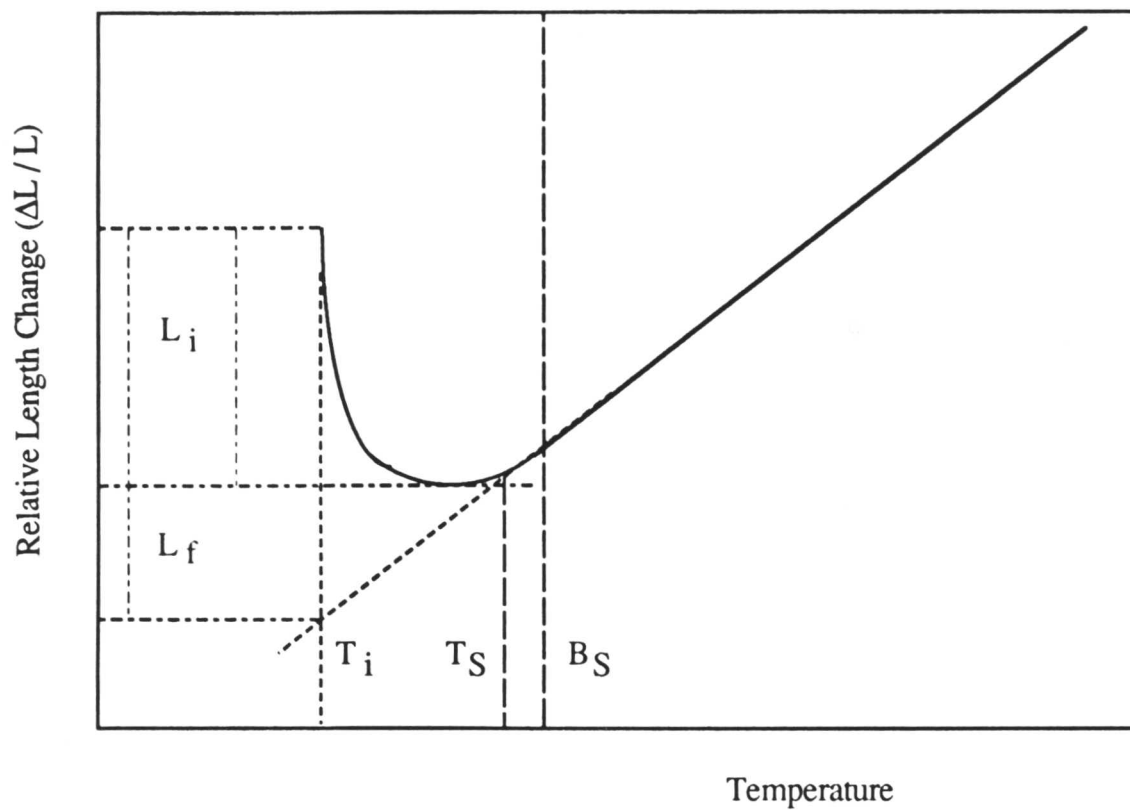


Fig. 4.9: Schematic representation of the method used to correct the dilatometry data to take into account of the transformation during cooling before reaching to the isothermal transformation T_γ . Note that this type of correction is valid only if no other reaction interfere the bainite transformation.

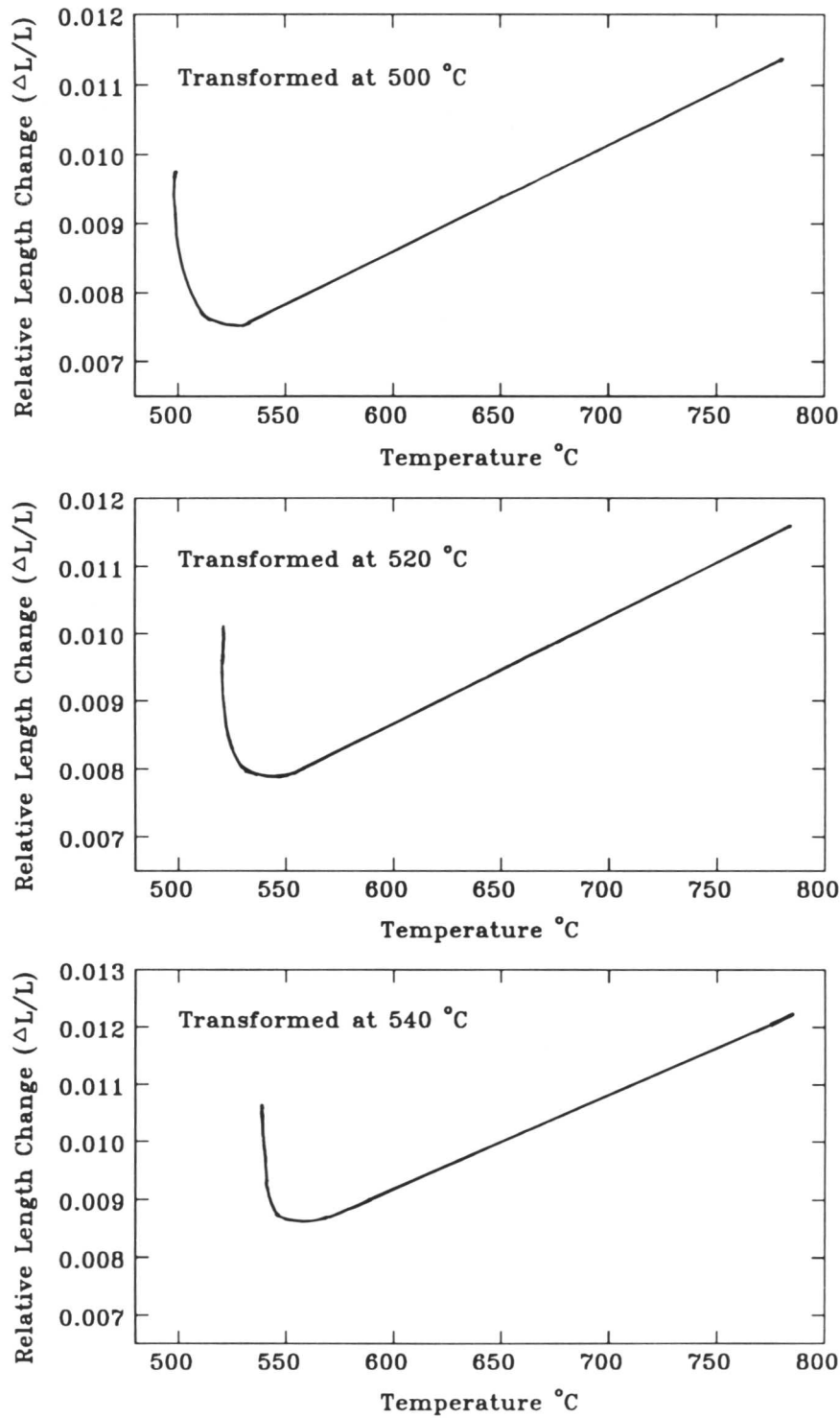


Fig. 4.10a: Temperature versus relative length change curves for the alloy A101, illustrating the transformation during cooling to the isothermal transformation temperature.

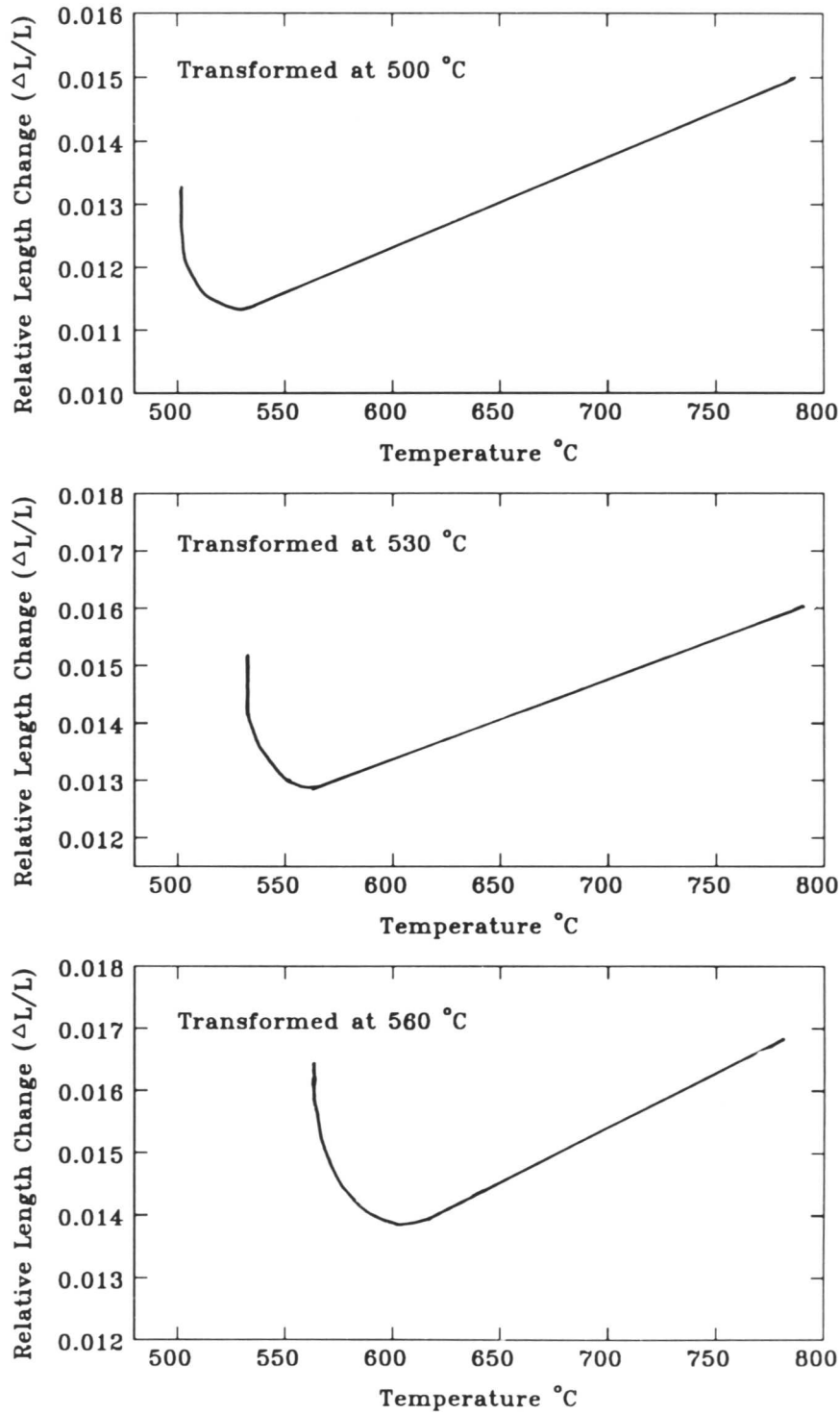


Fig. 4.10b: Temperature versus relative length change curves for the alloy A104, illustrating the transformation during cooling to the isothermal transformation temperature.

Table 4.5: *Original data and corrected data for alloys the A101, A103, and A104.*

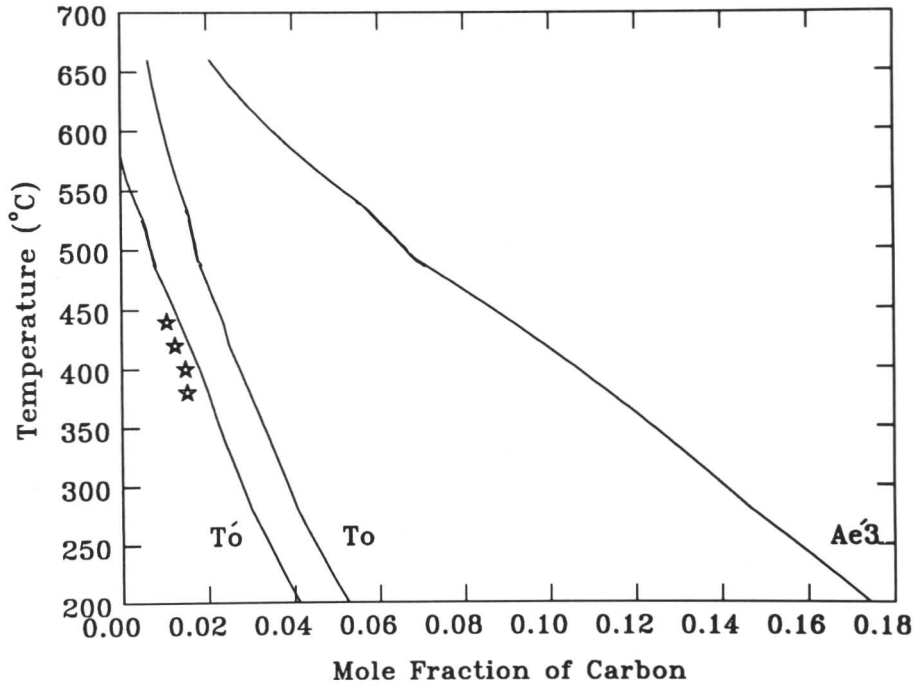
Temperature °C	Alloy No.	Original data ($\Delta L/L$)	Corrected data ($\Delta L/L$)
500	A101	0.00230	0.0029
520	A101	0.00235	0.0037
540	A101	0.00215	0.0034
500	A104	0.002	0.0024
530	A104	0.0023	0.0027
560	A104	0.00275	0.00374

4.7 Incomplete Reaction Phenomenon of Bainite

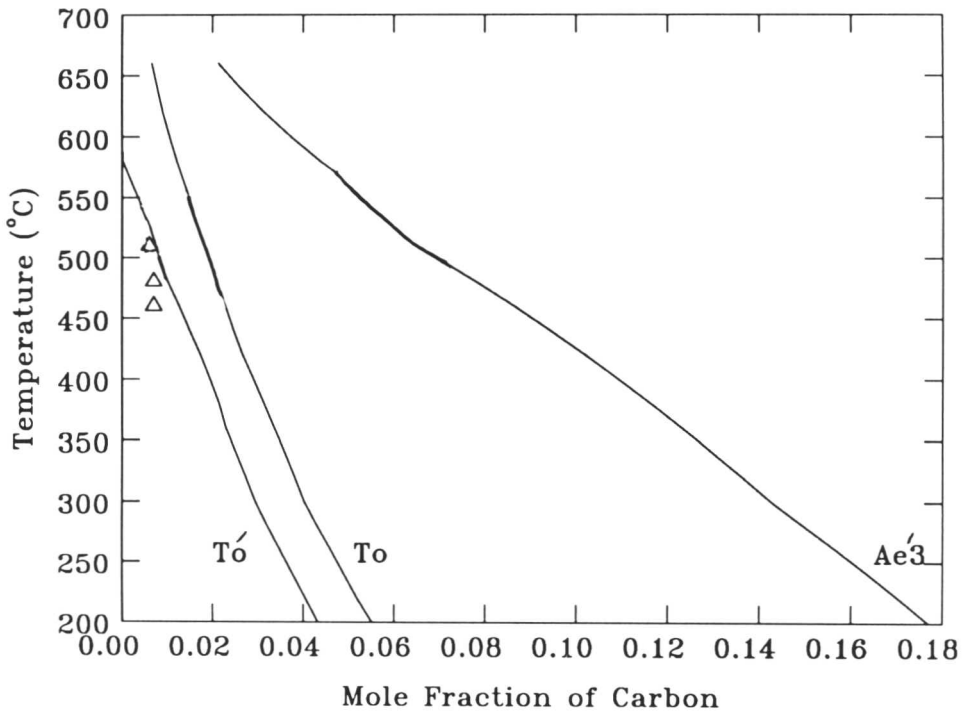
An interesting feature of bainite transformation is the existence of the “incomplete reaction phenomenon”. At any temperature within the bainite transformation range, and in the absence of any interfering secondary reactions, such as carbides or pearlite, only a limited quantity of bainitic-ferrite forms before the reaction terminates. This premature termination occurs before the carbon content of the remaining austenite reaches the equilibrium level indicated by the extrapolated Ae'_3 curve. The maximum extent of transformation that can be achieved increases with undercooling below the bainite-start (B_S) temperature.

It is apparent from Figs. 4.7 and 4.9, that in none of the present experiments did the volume fraction of bainitic ferrite exceed 0.4, the experiments can be interpreted [Bhadeshia *et al.* 1980] to be in agreement with the growth of bainite occurring by the propagation of martensitic sub-units, since the degree of transformation obtained complies approximately with T_0 or T'_0 curves.

The thermodynamic methods and data necessary for the calculation of Ae'_3 , T_0 and T'_0 curves have been described elsewhere [Aaronson *et al.* 1966; Shiflet *et al.* 1978; Bhadeshia and Edmonds, 1980] and the stored energy was taken to be 400 J mol⁻¹, according to Bhadeshia [1981]. The results are shown in Figs. 4.11 and 4.12. The experimental points refer to the carbon content of the residual austenite, following the rapid termination of the bainite reaction. They are calculated from the measured length changes by using Eq. 4.2. The Figs. 4.11 and 4.12 clearly indicate that the bainite reaction terminated before the carbon content of the residual austenite reaches the T'_0 , represents the maximum tolerable carbon use for the formation of fully supersaturated bainitic

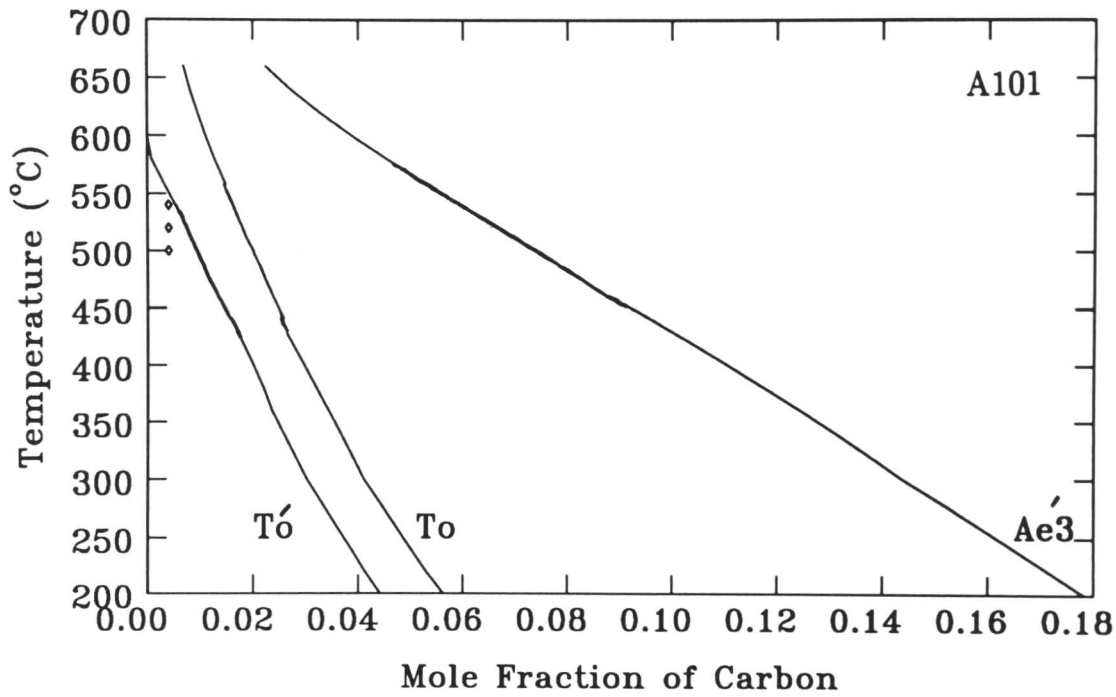


(a)

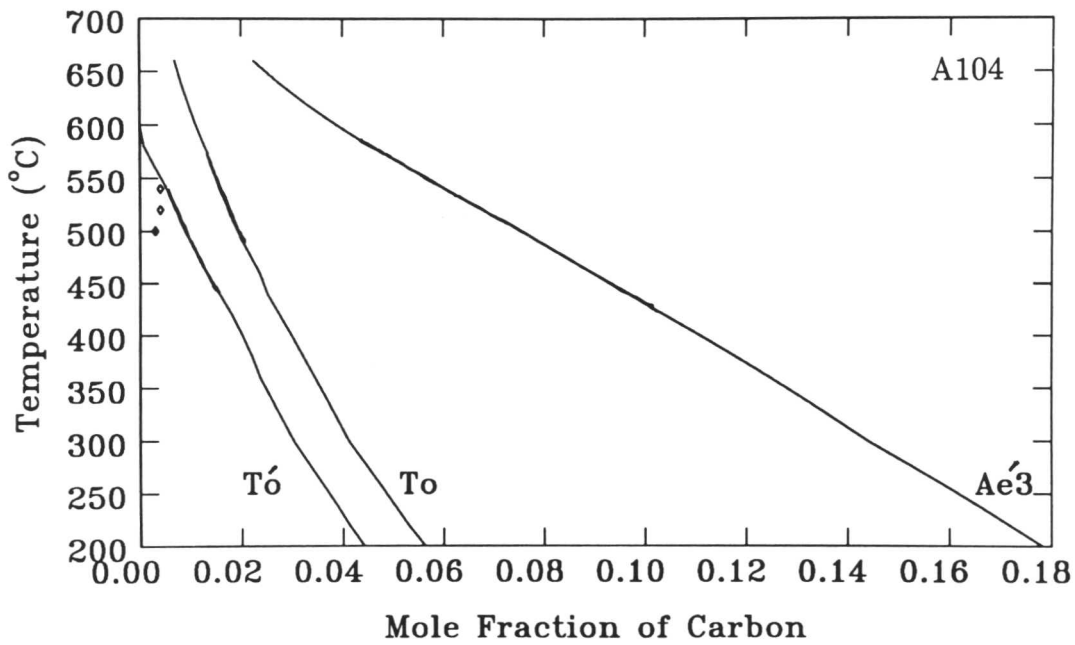


(b)

Fig. 4.11: Calculated phase diagram with experimental data of carbon content of austenite at the termination of isothermal bainite formation. (a) For alloy A2 and (b) For alloy A102. Note that the reactions stop well before Ae_3' curve.



(a)



(b)

Fig. 4.12: Calculated phase diagram with experimental data of carbon content of austenite at the termination of isothermal bainite formation. (a) For alloy A101 and (b) For alloy A104. Note that the reactions stop well before Ae₃' curve.

ferrite if the stored energy of bainitic ferrite taken into account. It is clear from the microstructures shown in Figs 4.6-4.9, that the extent of transformation is a sensitive function of temperature and this is totally characteristic of the incomplete reaction phenomenon [Hehemann, 1970]. This result together with the carbon content of austenite at the termination of bainite reaction are considered to be particularly relevant since there is no interference from carbide precipitation during the upper bainitic ferrite reaction in these alloys. Any precipitation of carbide would naturally reduce the carbon content of the enriched austenite, thereby promoting further transformation. Hence it can be concluded that the formation of bainite in the alloy studied follows an incomplete reaction phenomenon and confirms the results earlier investigations [Hehemann, 1970; Bhadeshia and Edmonds, 1979; 1980; Yang, 1987].

4.8 Surface Relief

Examination of a pre-polished, austenite and isothermally transformed specimens revealed that surface displacements could be associated with the upper bainite (Fig. 4.13). The uniformity of interference contrast on the tilted surfaces illustrated in Fig. 4.13, indicates that the invariant plane strain nature of the surface relief. Such displacements are characteristic of martensitic transformations and are taken to imply that the sub-units propagate in a displacive manner. This observation of an IPS shape change due to the formation of bainite has been noted by several other researchers [Ko, 1953; Cottrell and Ko, 1953; Bhadeshia and Edmonds, 1980]. This results is fully consistent with the sub-unit morphology and their martensitic growth.

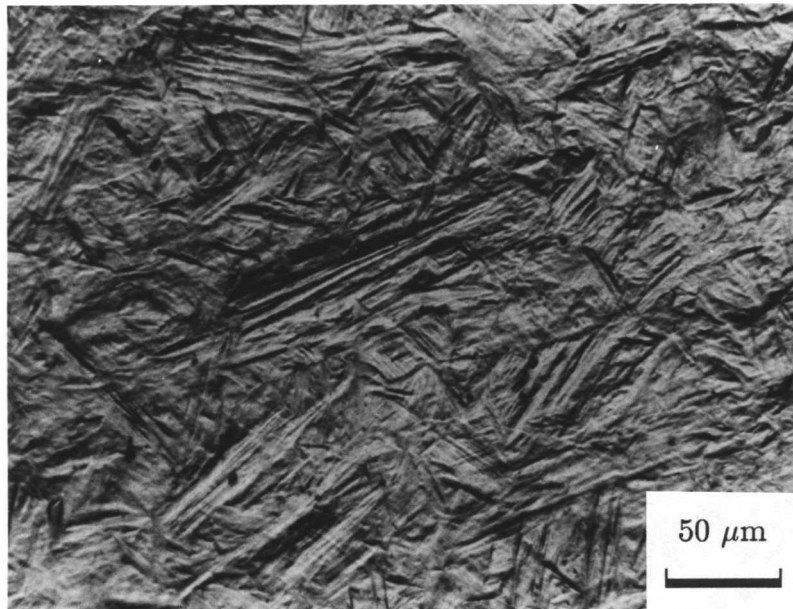
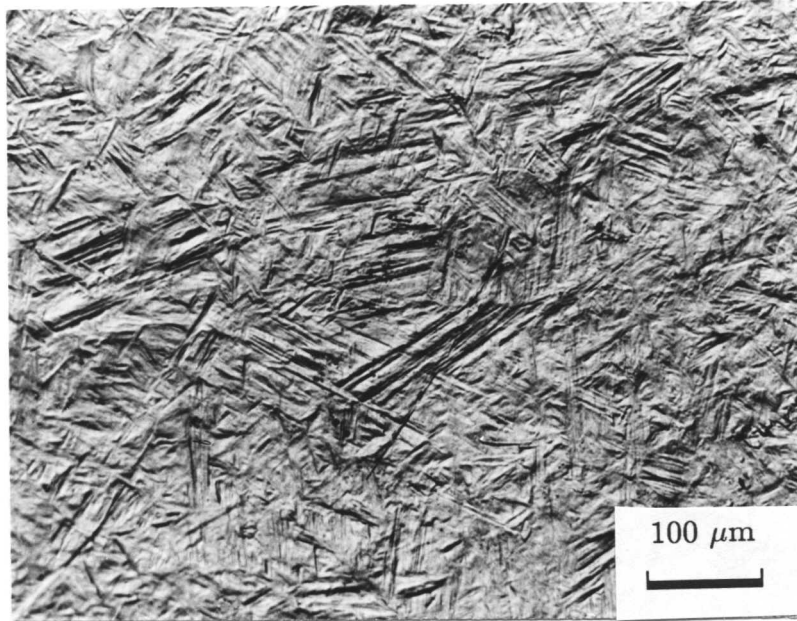


Fig. 4.13: *Micrographs showing the surface relief exhibited by bainite formation in alloy A2. Specimen isothermally transformed at 400 °C for 1000 s after austenitisation at 900 °C for 5 min.*

4.9 Conclusions

The austenite to bainite transformation has been studied in Fe-C-Si-Mn and Fe-C-Si-Ni steels used dilatometry backed by optical and transmission electron microscopy. It is concluded that:

- Bainite forms with a sheaf morphology and each sheaf consisting of ferrite sub-units.
- The sheaves nucleate at prior austenite grain boundaries and grow inwards of the grain.
- The maximum extent of bainite formation is dependent on transformation temperature below the B_S temperature.
- The reaction terminates prematurely well before the austenite carbon content reaches the Ae'_3 curve.
- The bainite formation terminate when the carbon content of residual austenite reaches at T'_0 .
- The bainite reaction follow an incomplete reaction phenomenon.
- Formation of bainite exhibit an IPS surface relief.

All these conclusions are consistent with the diffusionless displacive formation of bainite and the sub-unit morphology of bainite.



Chapter 5

TEMPERING OF BAINITE IN Fe-C-Si-Mn-Mo STEEL

Classically *tempering* is a process of reheating which is commonly applied in industry to martensitic steels in order to achieve required hardness and toughness properties. Tempering of bainitic microstructures is an important phenomenon from an industrial point of view both for wrought steels and for weld deposits. Many steel assemblies in power generation plant operate at 565 °C and these service conditions cause the tempering of the initial microstructure, which usually consists of a mixture of allotriomorphic ferrite and bainite [Bhadeshia, 1988]. It has been demonstrated by Irvine and Pickering [1960] that bainitic steels also show an improved combination of mechanical properties after tempering. In multilayered weld deposits, tempering and reaustenitisation are inevitable because the deposition of every new layer reheats those deposited previously. Weld microstructures often contains substantial quantities of intragranularly nucleated bainite, the so-called acicular ferrite. Therefore, the tempering process is equally important to weld deposits.

All these examples emphasise the importance of the tempering process and although a large amount of data are available on the tempering of quenched steels [Baker and Nutting, 1959; Irani and Honeycombe, 1955; Ohmori, 1972; Speich and Leslie, 1972], relatively little attention has been given to the tempering of bainite. The following chapter deals with a detailed microstructural analysis of tempering of bainite in an ultra high strength steel containing a strong carbide forming element Mo. This study implements some earlier work on a Fe-C-Si-Mn alloy by including the effect of alloy carbide formation. Particular attention is also given to see the effect of tempering on bainite morphology.

5.1 Experimental Procedures

The chemical composition of the steel selected for the present study has been given in Table 3.1 and designated as alloy A2. The steel was received in the form of 10 mm diameter bar, from which 3 mm diameter rods were prepared by swagging treatments[§]. All specimens were homogenised at 1200 °C for three days in vacua and Ni-plated to avoid surface degradation during the subsequent heat treatments. A Theta Industries high speed dilatometer was employed for short time (< 16 hours) tempering, while for longer time tempering, electrical resistance heating furnaces

[§] The details of specimen preparation and experimental techniques have been described in Chapter 3.

were used. Fig. 5.1 shows schematically the heat treatment cycles used throughout the present study.

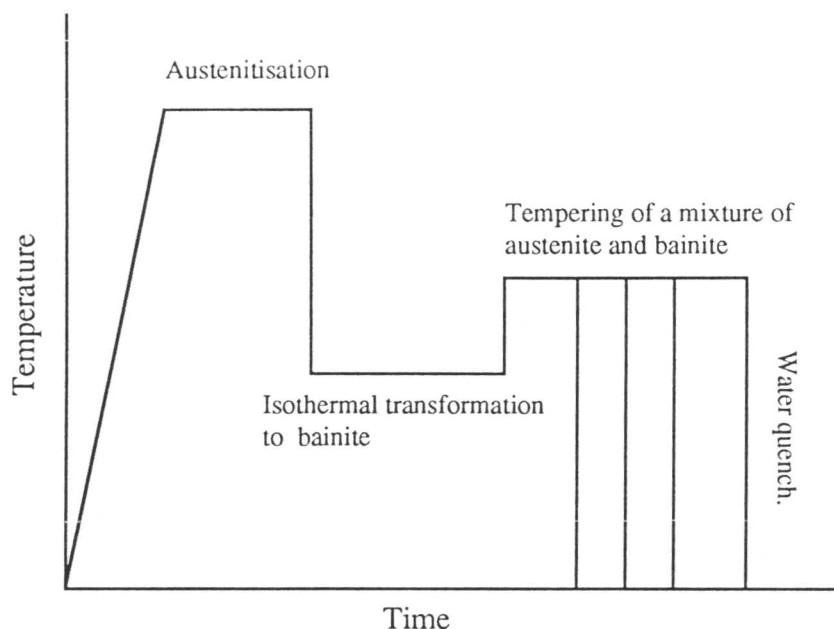


Fig. 5.1: Schematic representation of the heat treatment cycles used for the tempering of bainite.

The specimens were transformed to bainite at 400 °C and then rapidly heated to a higher tempering temperature *i.e.*, 620 °C, instead of quenching to ambient temperature. This avoids the formation of any martensite during cooling to ambient temperature.

The selection of the tempering temperature was critical because the purpose of tempering was to decompose the austenite. The tempering temperature must therefore be below the reaustenitisation temperature, which was determined to be about 660 °C using dilatometry (see Chapter 11 for details).

Thin foils were obtained from the heat treated samples by the methods described in Chapter 3. In order to follow up the precipitation sequence carbon

extraction replicas were prepared using the method of Smith and Nutting [1957] as described in Chapter 3. Both thin foils and carbon extraction replicas were examined in a PHILIPS 400T transmission electron microscope operating at 120 kV and attached with an energy dispersive x-ray spectrometer to facilitate EDX analysis. Specimens for optical microscopy were prepared by conventional metallography techniques. The hardness was measured on a Vicker's hardness machine.

5.2 Results and Discussion

The microstructure observed after isothermal transformation to bainite is shown in Fig. 5.2.

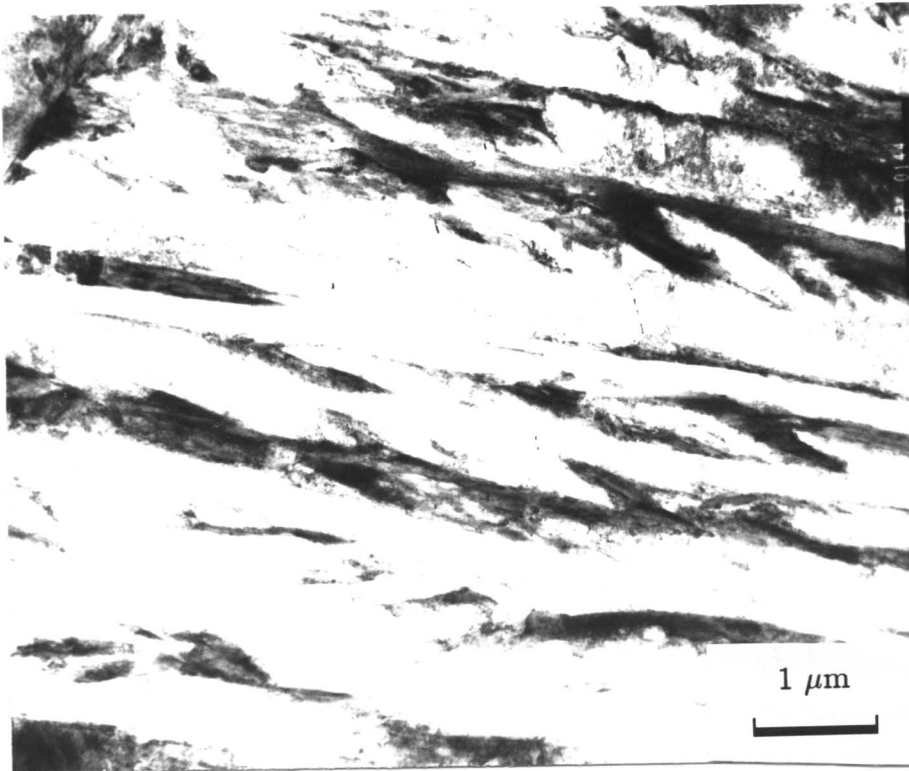
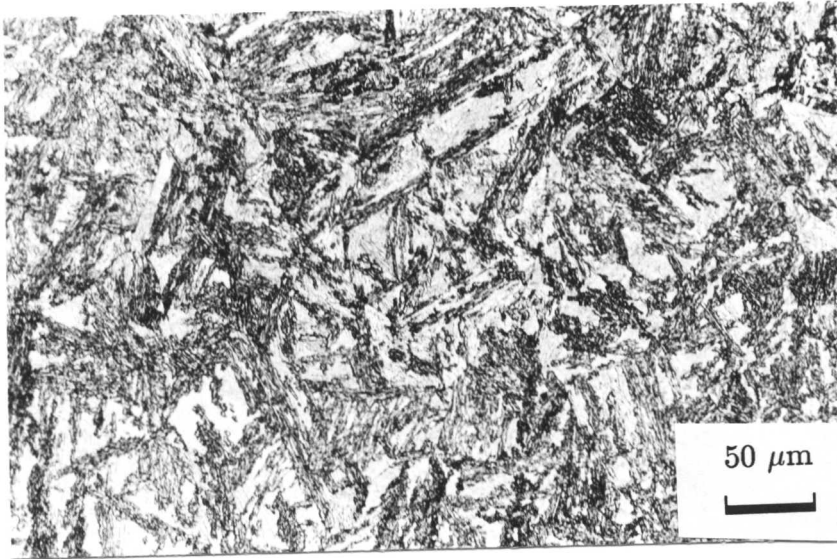


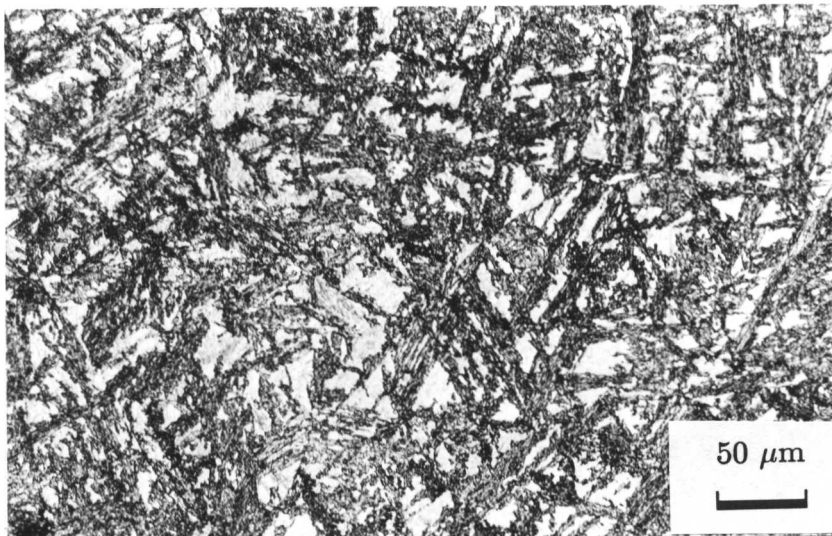
Fig. 5.2: *TEM micrographs showing bainite microstructure, specimen austenitised at 900 °C for 5 min and isothermally transformed at 400 °C for 1000 s.*

5.2.1 TEM Study of Tempered Bainite

Optical microscopy (Fig. 5.3) did not reveal any clear changes in microstructure during the early stages of tempering, although a comparison of the samples tempered for 2000 s and 5 days shows changes in contrast. Attention was therefore focused on transmission electron microscopy, the as-transformed (untempered) microstructure being illustrated in Fig. 5.4.

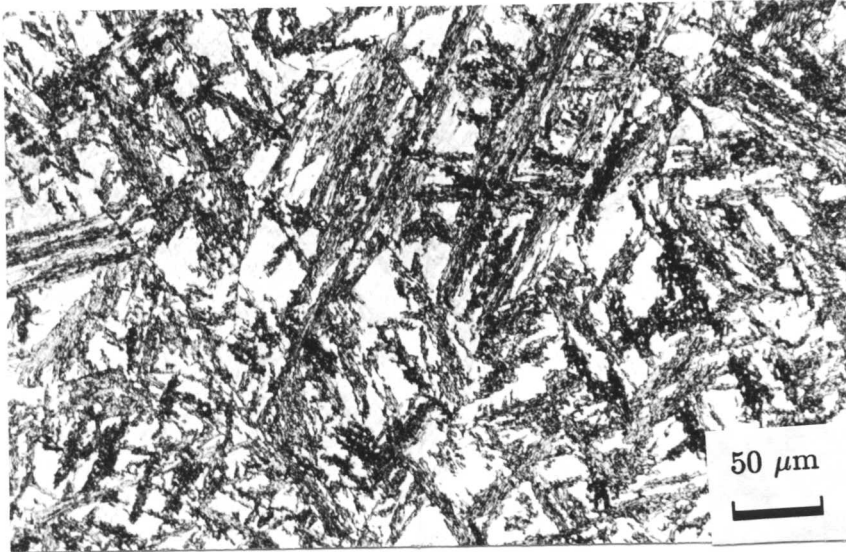


(a) Tempered for 2000 s.

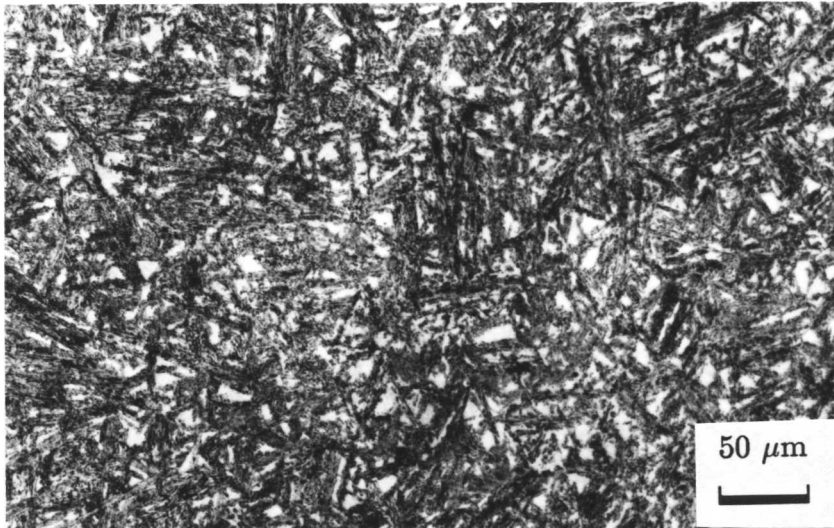


(b) Tempered for 4000 s.

Fig. 5.3: *Continued.....*

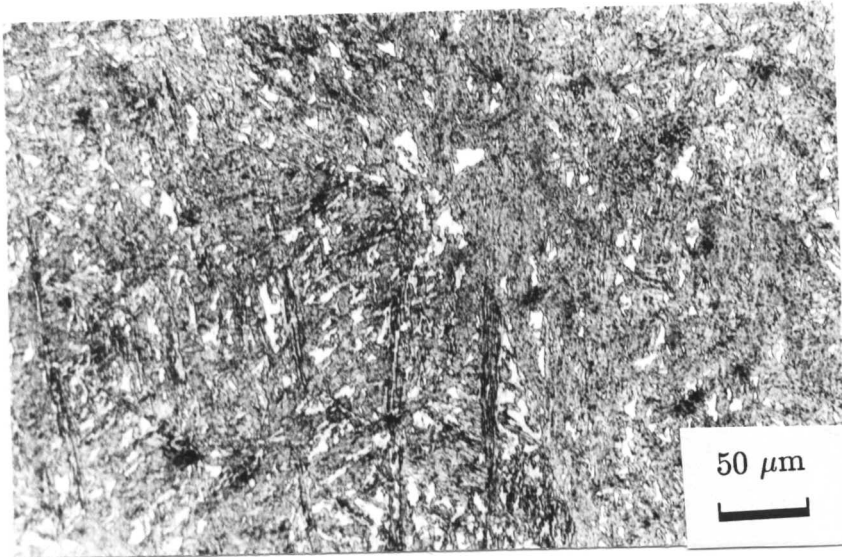


(c) Tempered for 8000 s.

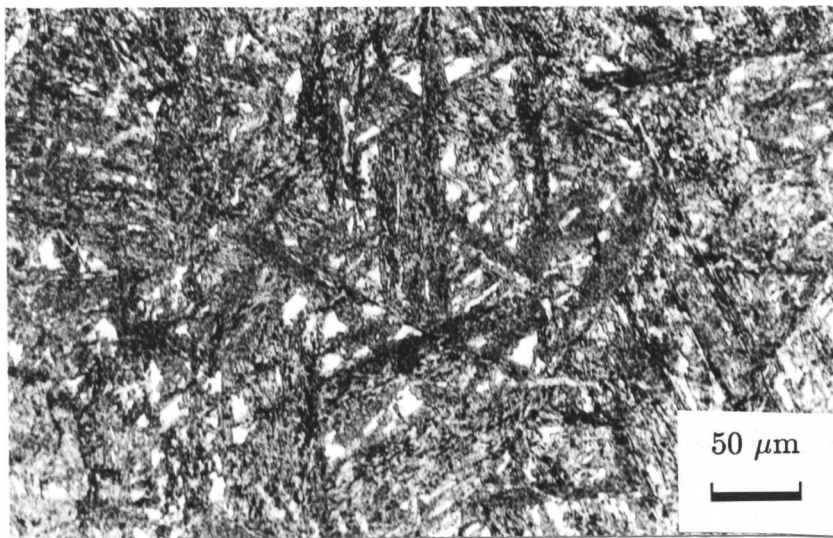


(d) Tempered for 16 hr.

Fig. 5.3: *Continued.....*



(e) Tempered for 2 days.



(f) Tempered for 5 days.

Fig. 5.3: Optical micrographs showing the effect of tempering time on the microstructure. All specimens were austenitised at 900 °C for 5 min, transformed to bainite microstructure at 400 °C for 1000 s and tempered at 620 °C.

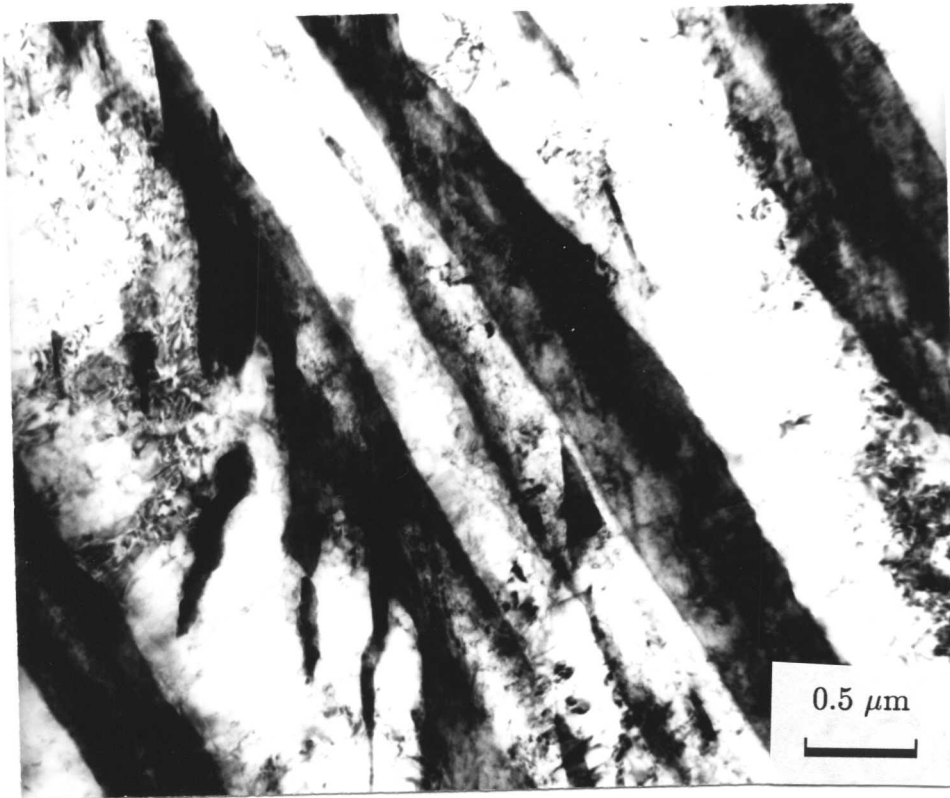
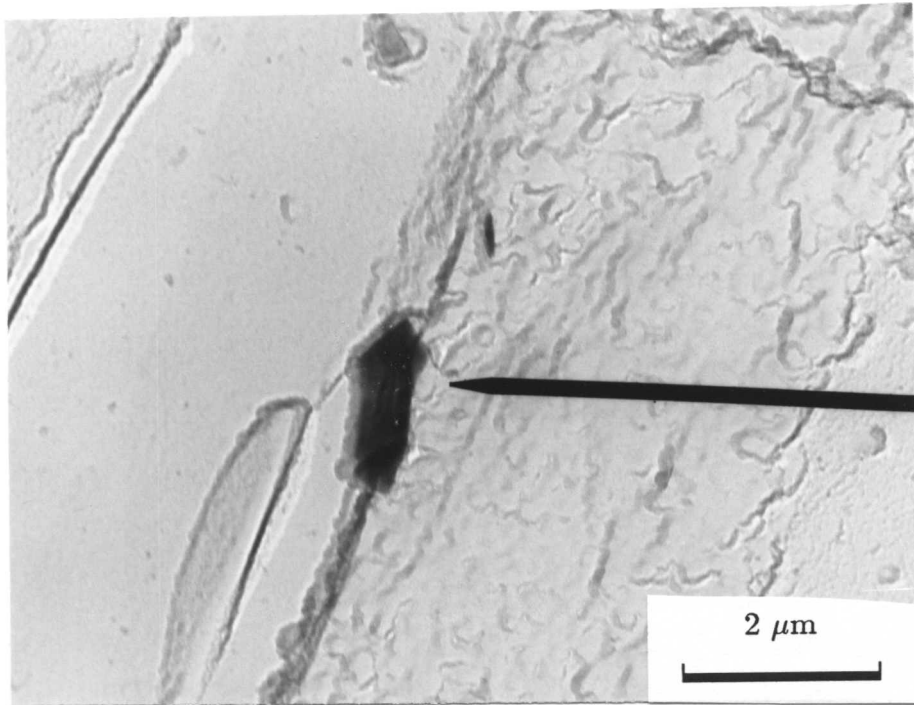


Fig. 5.4: *TEM thin foil micrograph showing bainite sheaves microstructure. Note the lenticular-plate morphology of bainitic ferrite sub-units, particularly the curved tip due to the constraint imposed by the matrix.*

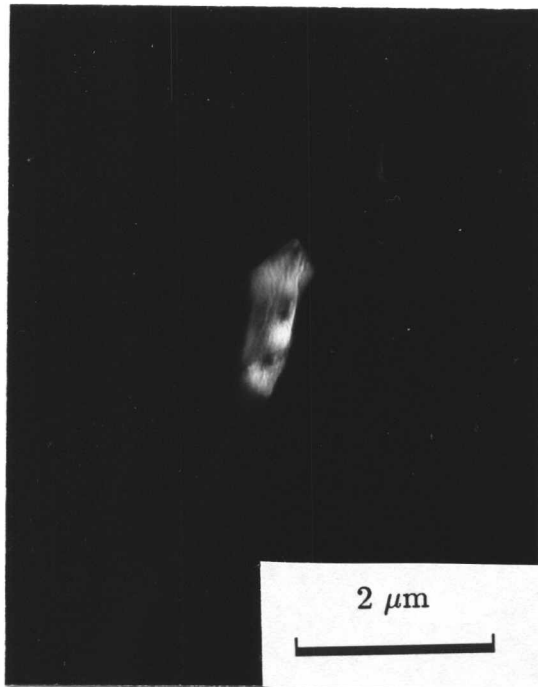
5.2.2 Precipitation of Carbides During the Tempering of Bainite

The formation of bainitic ferrite leads to an increase in the carbon concentration of the austenite which remains untransformed. The austenite eventually began to decompose to a mixture of carbides and ferrite. The precipitation process started first at the prior austenite/bainitic ferrite boundaries, as shown in Fig. 5.5. These precipitates identified as cementite by electron diffraction (Figs. 5.5, 5.6).

Microanalysis results on extracted carbides also demonstrate that their compositions were consistent with cementite (Table 5.2). More profuse precipitation followed prolonged tempering, but during these relatively early stages of tempering the carbide phase was identified to be rod-like cementite (Fig. 5.5). Fig. 5.6 shows that many of the carbides precipitated from the austenite films trapped between the bainitic ferrite sub-units, so that the decomposition of the austenite did not lead to any change in the bainitic ferrite plate shape, presumably because the carbides pin the sub-unit boundaries. The strong alignment of the carbides along the sub-unit boundaries is obvious in Fig. 5.6b, where the directions along which the carbides precipitate most preferably are seen to vary with the sheaf (and hence austenite films) orientation. Although the majority of carbides were identified clearly to be cementite (Fig. 5.7b, c), classical needle like Mo_2C precipitates were also detected after 4000 s at 600 °C (Fig. 5.7d, e). The composition of these particles is also consistent with molybdenum rich particles (Table 5.2).



(a)

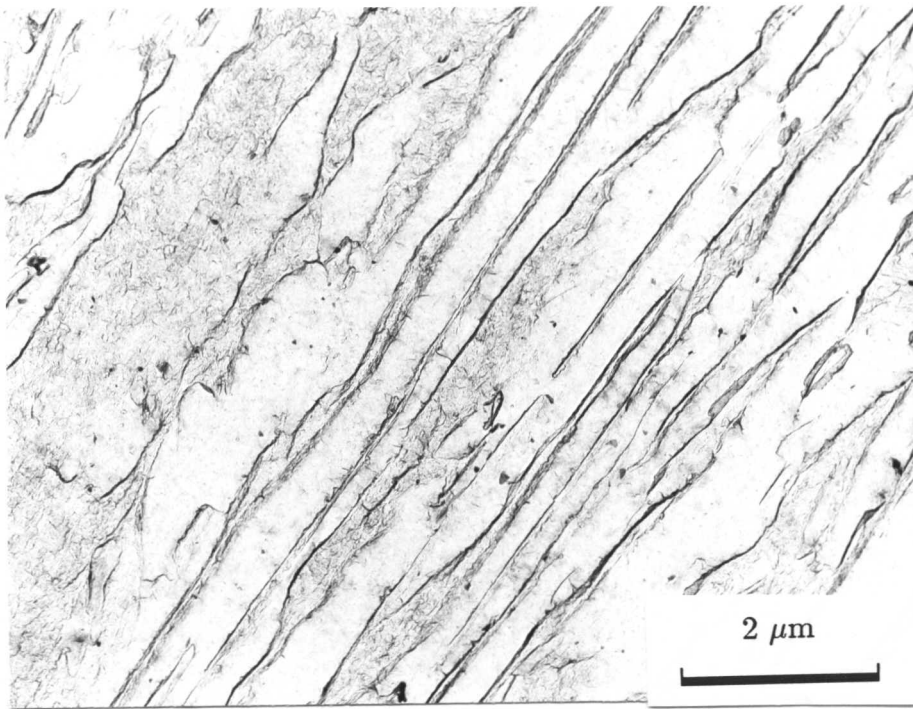


(b)

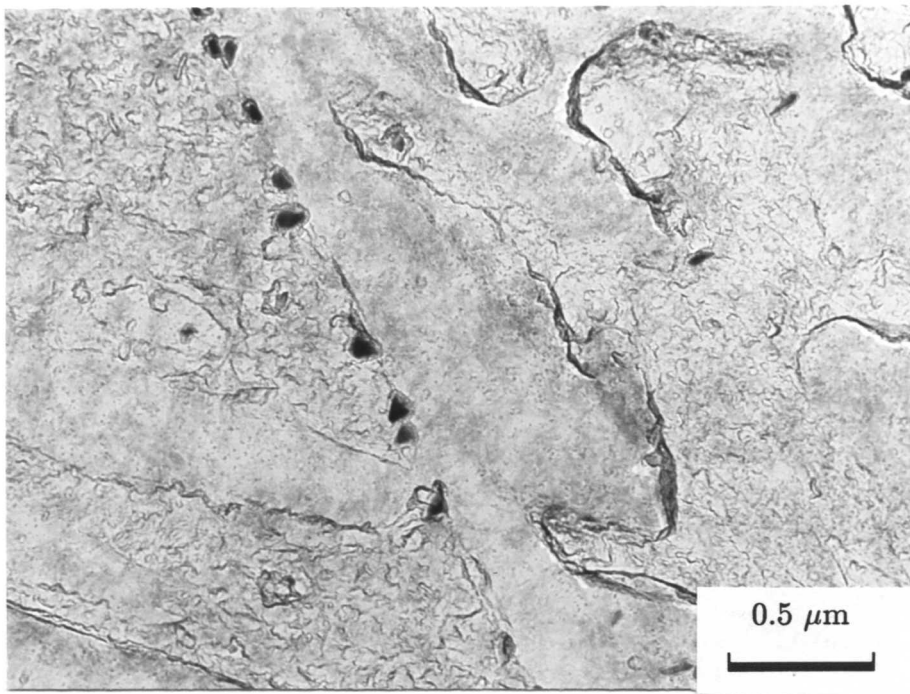


(c)

Fig. 5.5: Carbon extraction replica micrographs showing the identification of grain boundary carbide precipitate in specimen tempered at 600 °C for 2000 s. (a) Bright field, (b) dark field and (c) corresponding selected area diffraction pattern.

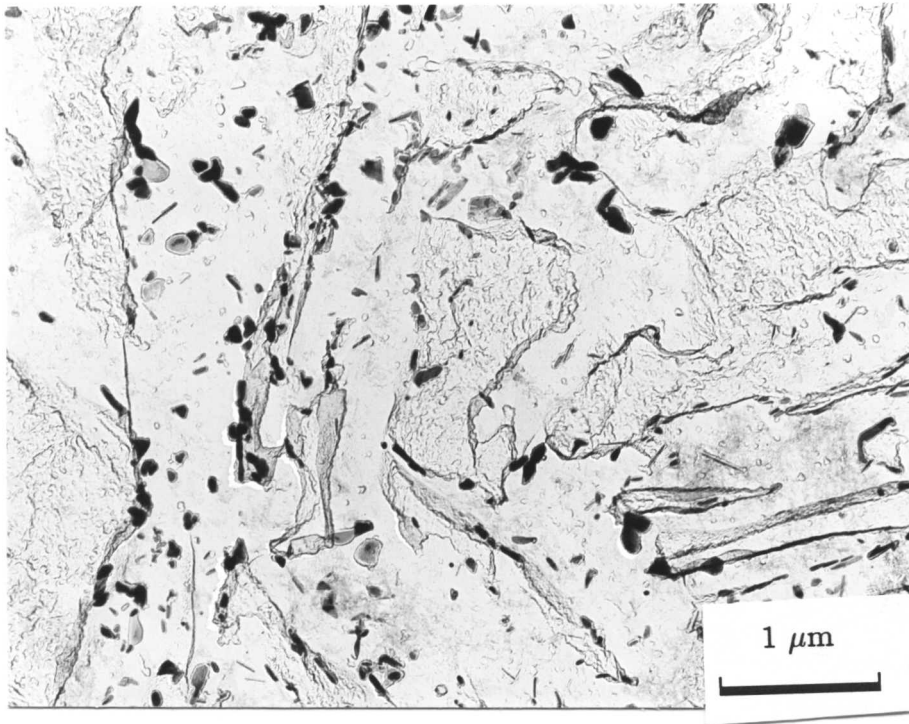


(a)

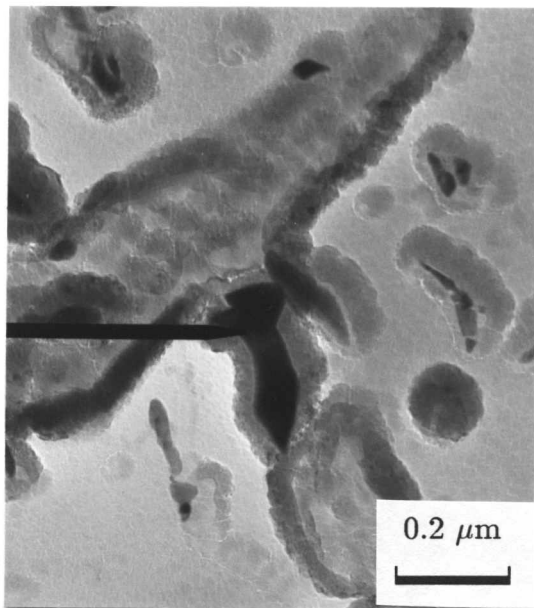


(b)

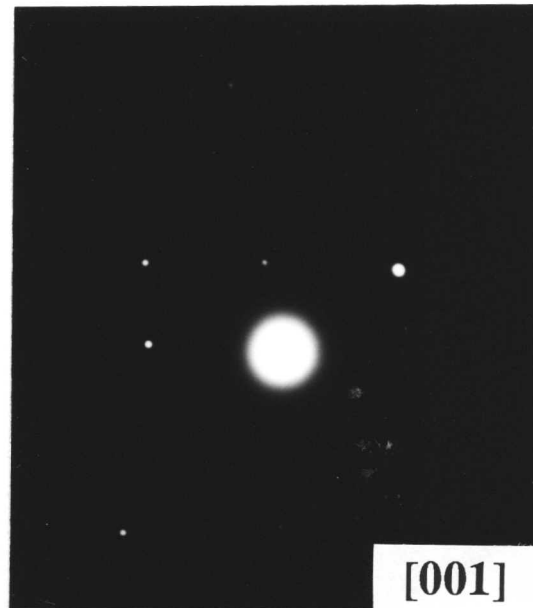
Fig. 5.6: *Replica electron micrograph showing that precipitation of cementite after 2000 s of tempering at 600 °C. Most of the carbides formed at the prior austenite boundaries.*



(a)



(b)



(c)

Fig. 5.7: *Continued*

The molybdenum content of the carbides appeared to increase with tempering time although this would have to be confirmed by more experiments. The number density of Mo_2C type precipitates increased with further tempering, at the expense of cementite (Fig. 5.8).

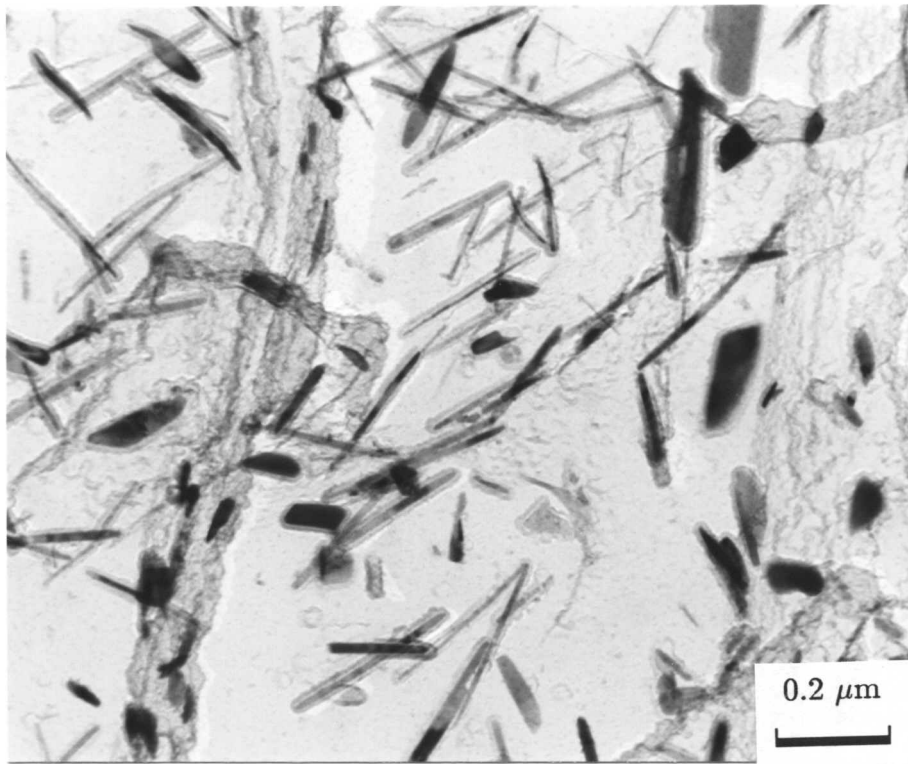
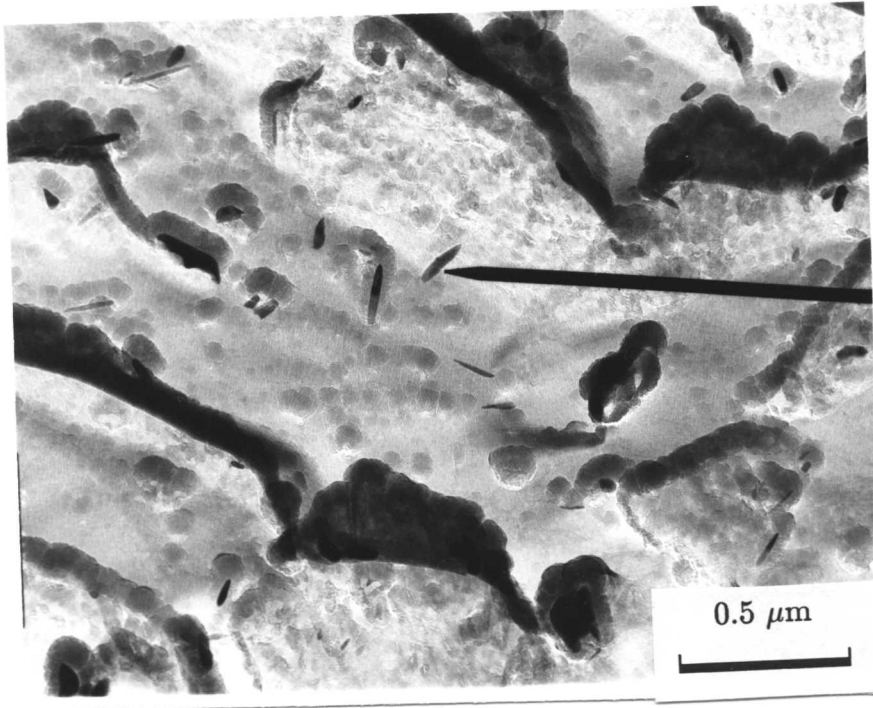


Fig. 5.8: *Micrograph showing substantial nucleation of Mo_2C precipitate within bainitic ferrite in specimen tempered for 8000 s at 600 °C.*



(d)



(e)

Fig. 5.7: (a) Replica electron micrograph showing the precipitation of Fe_3C after 4000 s of tempering at $600\text{ }^\circ C$. (b) Bright field from a Fe_3C particle and (c) corresponding diffraction pattern. (d) Bright field of a Mo_2C precipitate and (e) corresponding diffraction pattern.

Some M_6C carbide was also found to form after prolonged annealed (Fig. 5.9), the M_6C have a lower molybdenum concentration relative to the Mo_2C .

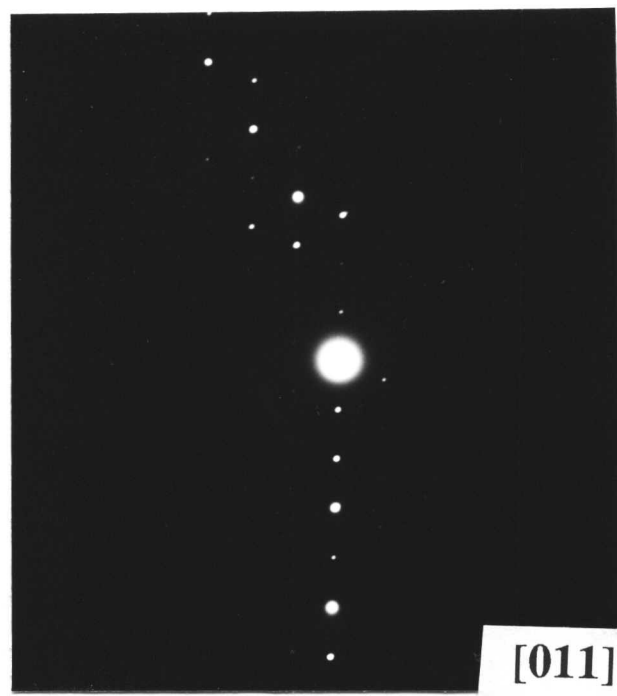
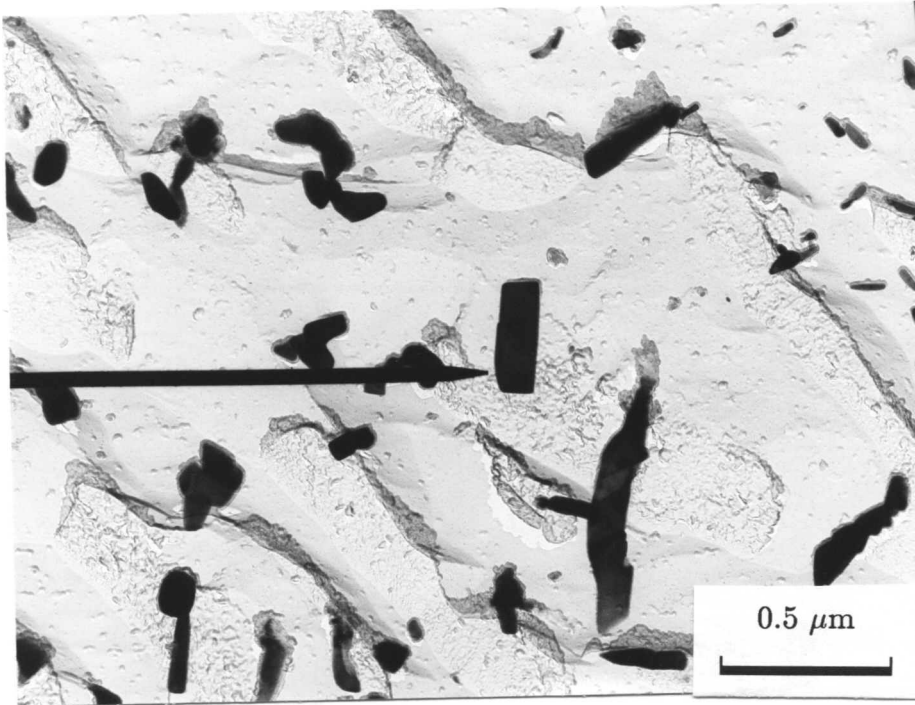


Fig. 5.9: Carbon extraction replica micrograph and corresponding diffraction pattern of a M_6C precipitate in specimen tempered at 600 °C for 16 hr.

5.2.3 Microanalysis of Precipitates

The identification of carbides were carried out using EDX X-ray analysis and selected area electron diffraction patterns. For this purpose a large number of electron diffraction patterns were taken and indexed to characterise the crystal structures of carbides. Chemical compositions of the precipitates were determined using energy dispersive X-ray analysis carried on carbon extraction replicas. These are given in Table 5.1 as a function of time. It can be seen that accelerating tempering has produced considerable variations in the compositions of the carbides.

Table 5.1: *Chemical composition of carbides determined by using energy dispersive X-ray analysis as a function of tempering time all specimens tempered at 620 °C.*

Tempering Time	Chemical Composition (wt. %)			Precipitate
	Fe	Mn	Mo	
2000 s	93.4	6.54	0.06	Fe ₃ C
2000 s	68.57	31.13	0.29	Fe ₃ C
4000 s	64.55	<0.1	35.45	M ₆ C
4000 s	93.45	6.54	<0.1	Fe ₃ C
4000 s	32.25	5.55	62.19	Mo ₂ C
4000 s	99.2	0.25	0.55	Fe ₃ C
8000 s	17.87	<0.1	82.13	Mo ₂ C
8000 s	82.49	17.51	<0.1	Fe ₃ C
16 hr	35.06	3.02	61.91	M ₆ C
16 hr	48.05	12.54	39.42	M ₆ C
16 hr	37.6	3.15	59.25	M ₆ C
16 hr	2.09	2.344	96.58	Mo ₂ C
31 days	58.80	35.80	5.92	Fe ₃ C
31 days	28.33	4.58	67.10	Mo ₂ C
31 days	5.12	2.41	92.40	Mo ₂ C
31 days	26.92	8.21	64.87	M ₆ C
31 days	56.92	34.78	8.312	M ₆ C

5.2.4 Effect of Tempering Time on Sub-Unit Morphology

Fig. 5.10-14. illustrate the effect of tempering time on the shape of the bainitic ferrite sub-unit. Fig. 5.10a shows the nucleation of bainite sheaves from the prior austenite grain boundary. It can be seen from the micrographs in Fig. 5.10 that there is some tendency for “spheroidisation” after tempering for 2000 s; the tips of the ferrite sub-units beginning to become round.

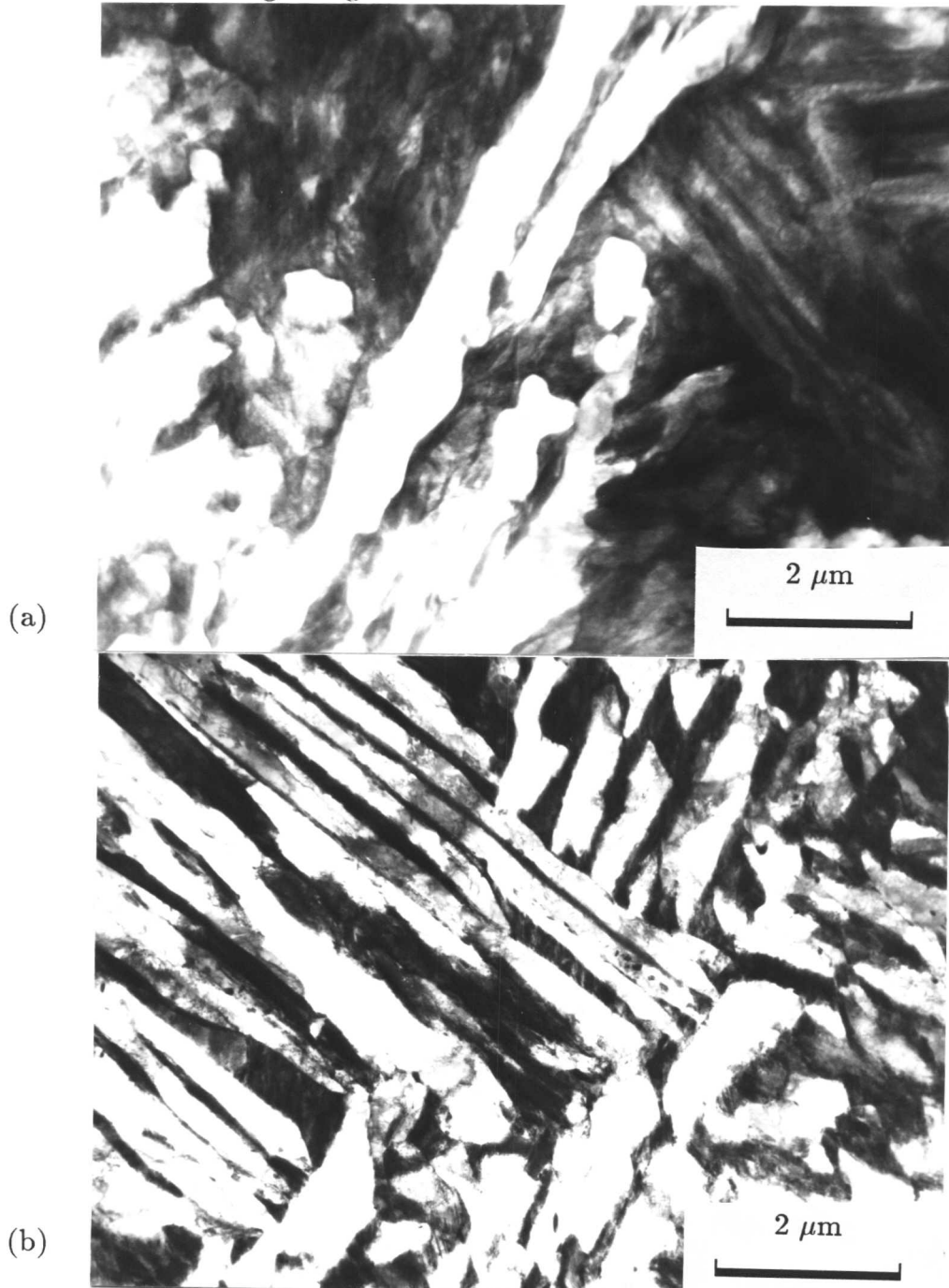


Fig. 5.10: TEM micrographs showing the effect of short time tempering on the ferrite sub-units. (a) Tempered at 600 °C for 2000 s. (b) Tempered at 600 °C for 4000 s.

Prolonged annealing continues to produce spheroidisation, as illustrated in Figs. 5.13 and 5.14. It can be seen from the micrograph that the original lenticular sub-unit morphology with fine tips essentially disappears although a slab shape of ferrite is still maintained. There is some evidence of sub-unit coalescence (Fig. 5.11b); such coalescence seems to occur most rapidly within a given sheaf, presumably because the sub-units are all interconnected even before annealing. While the broad faces of these sub-units still retain their plate-like shape and this characteristic remains unchanged during tempering for periods of upto 7 days. After that “recrystallisation” started (Fig. 5.13a). It can be observed from the micrograph in Fig. 5.13, that the ferrite formed as result of the decomposition of residual austenite recrystallised first (Fig. 5.13a), while the bainitic ferrite sub-units still retain their parallelism (Fig. 5.13c), but they were ultimately recrystallised after long time *i.e.*, 31 days of tempering (5.14).

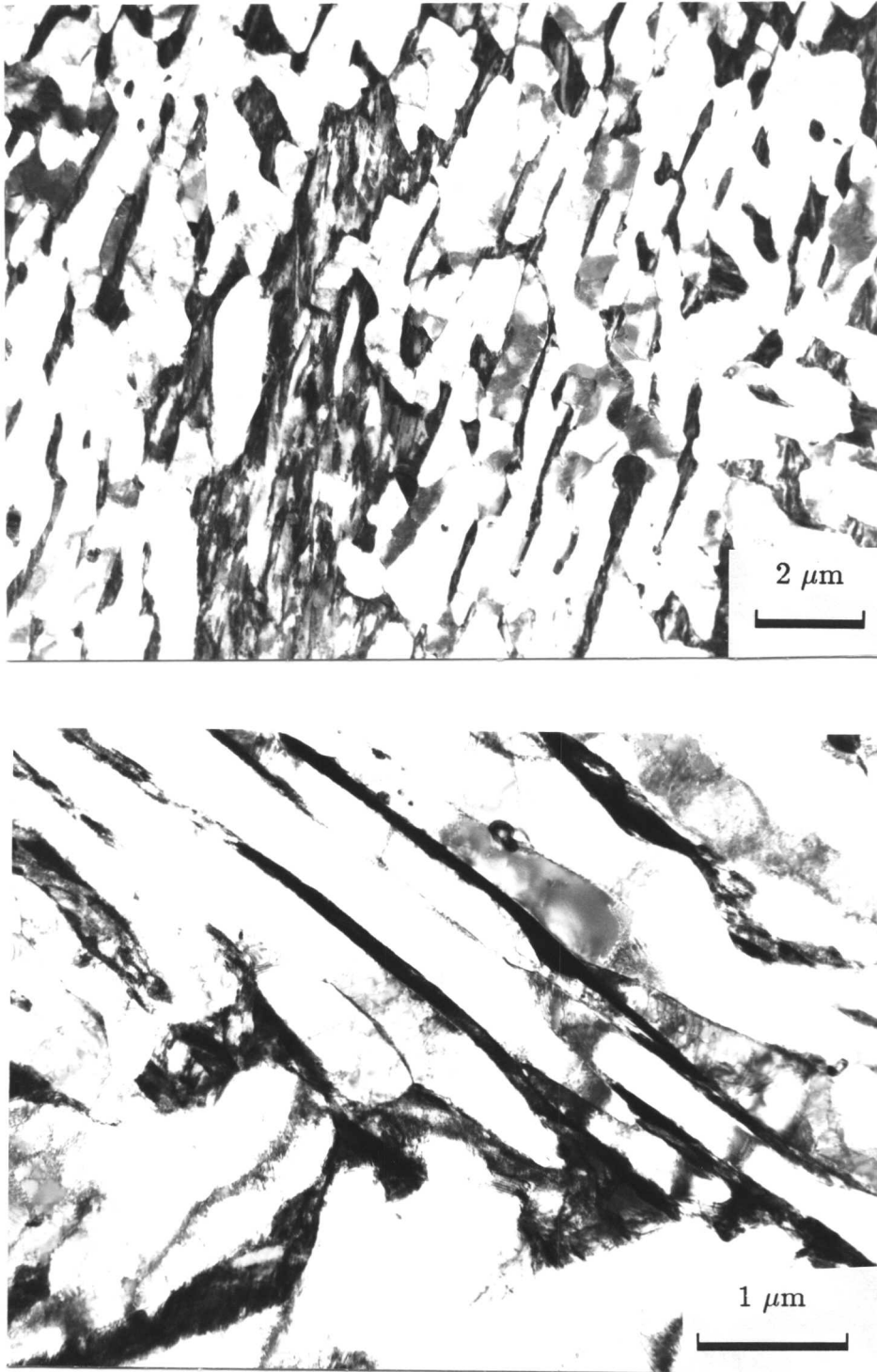


Fig. 5.11: TEM thin foil micrographs showing change in ferrite sub-units morphology after tempering for 16 hr at 600 °C. The tips of the sub-units have spheroidised, while their broad faces have altered little and remain more or less parallel to each other.

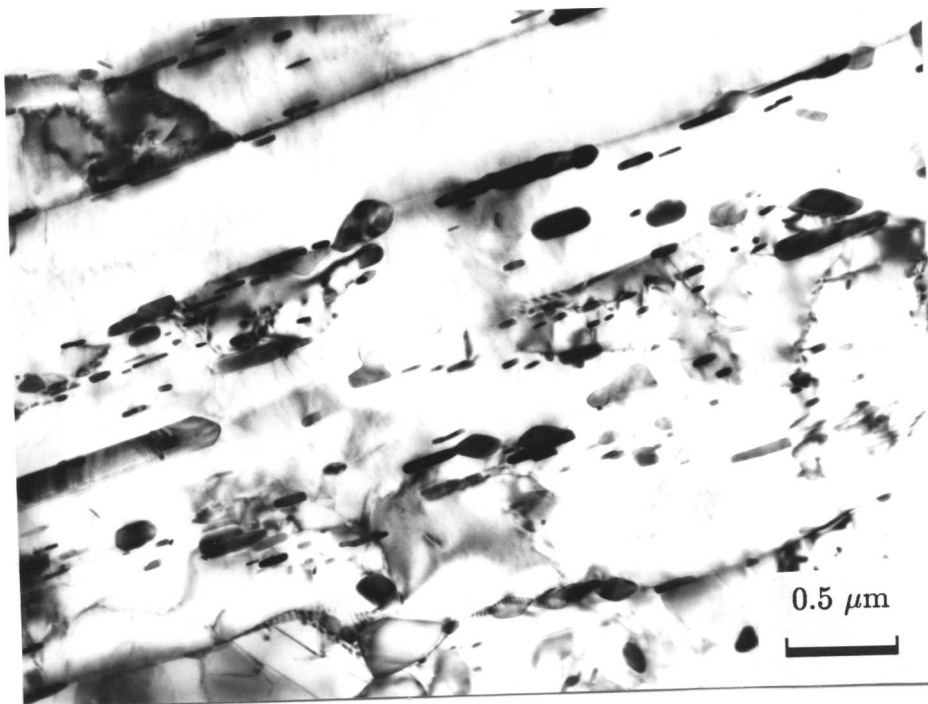
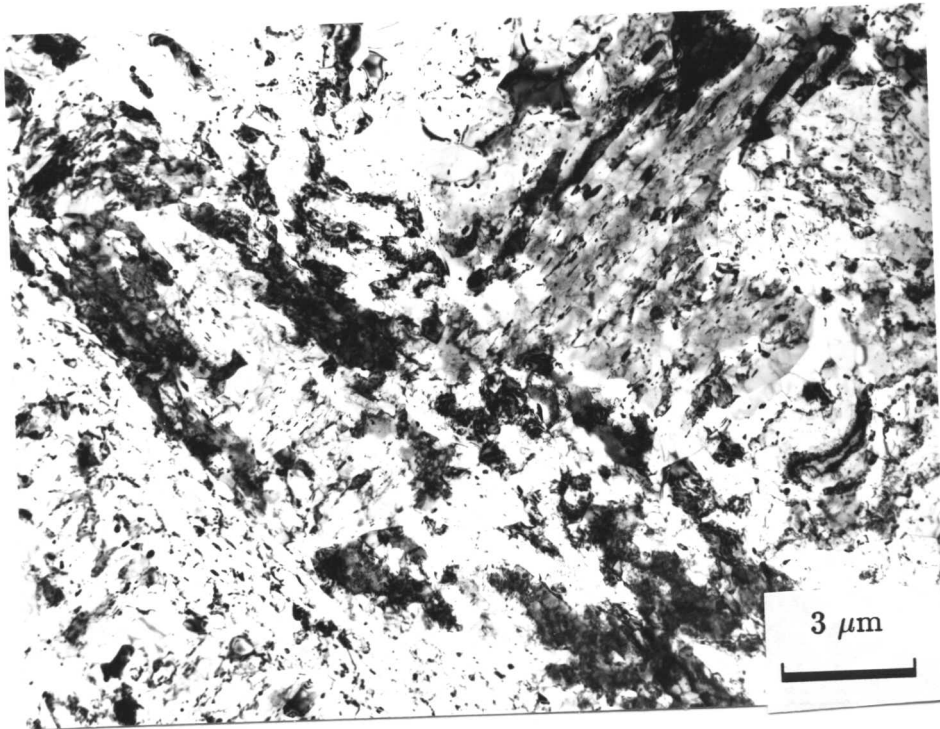


Fig. 5.12: *Micrographs showing microstructure of specimen tempered for 7 days at 600 °C. Note that the ferrite sub-units spheroidised but the broad faces still retained their parallel formation.*

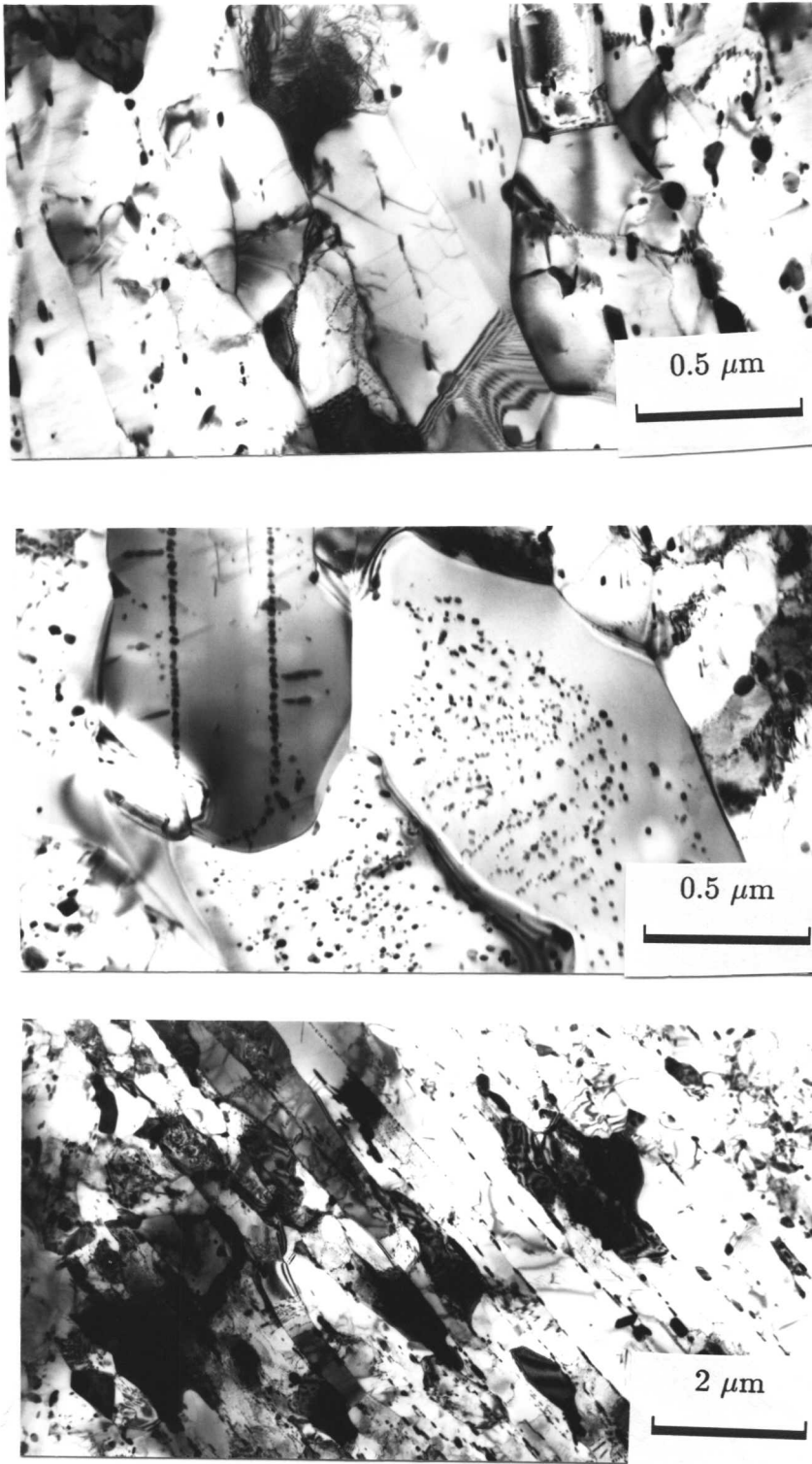


Fig. 5.13: TEM micrographs showing that specimen partially recrystallised after 18 days of tempering at 600 °C. The ferrite formed as result of tempering of martensite recrystallised, while the sub-units of bainitic ferrite still retained their parallel formation.

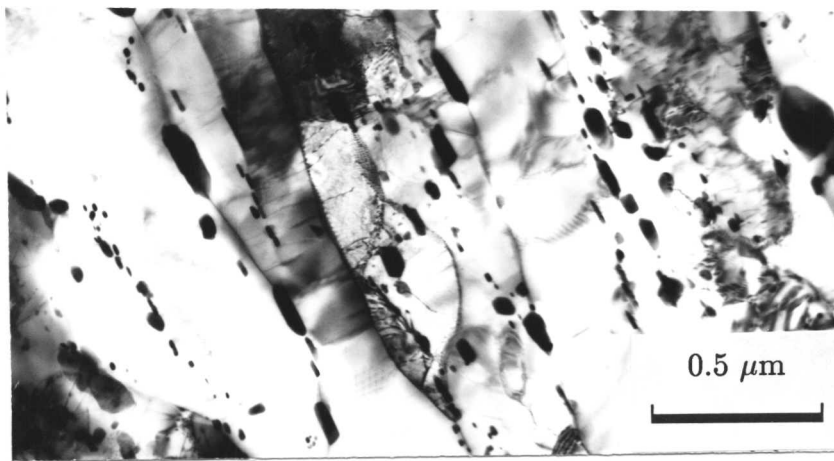
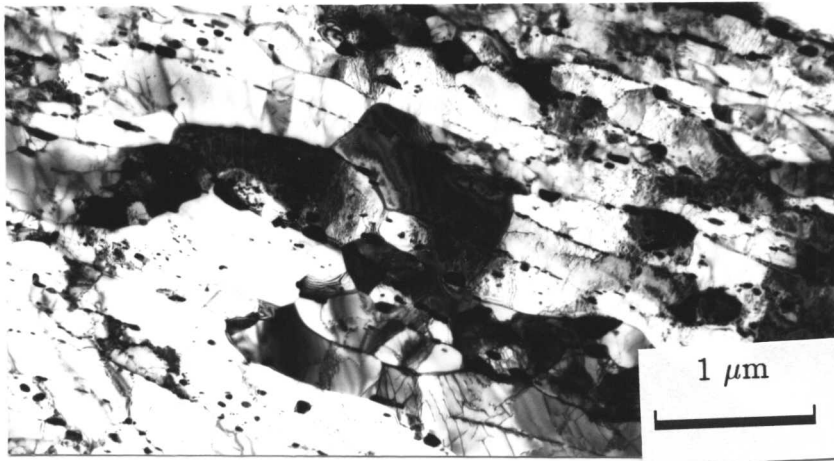


Fig. 5.14: *Recrystallised microstructure observed in specimen after 31 days of tempering at 600 °C, TEM thin foil micrographs.*

5.2.5 Decomposition of Retained Austenite

It was surprising to find that some of the original austenite remained untransformed even after annealed at 620 °C for 7 days. This undecomposed austenite transforms to the highly twinned martensite; Fig. 5.15 is a micrograph of the specimen tempered for 7 days at 620 °C, showing the twinned martensite that forms during quenching to ambient temperature. This might have originally been a larger region of relatively low carbon austenite, in which case it would be difficult for it to decompose by the precipitation of carbides.

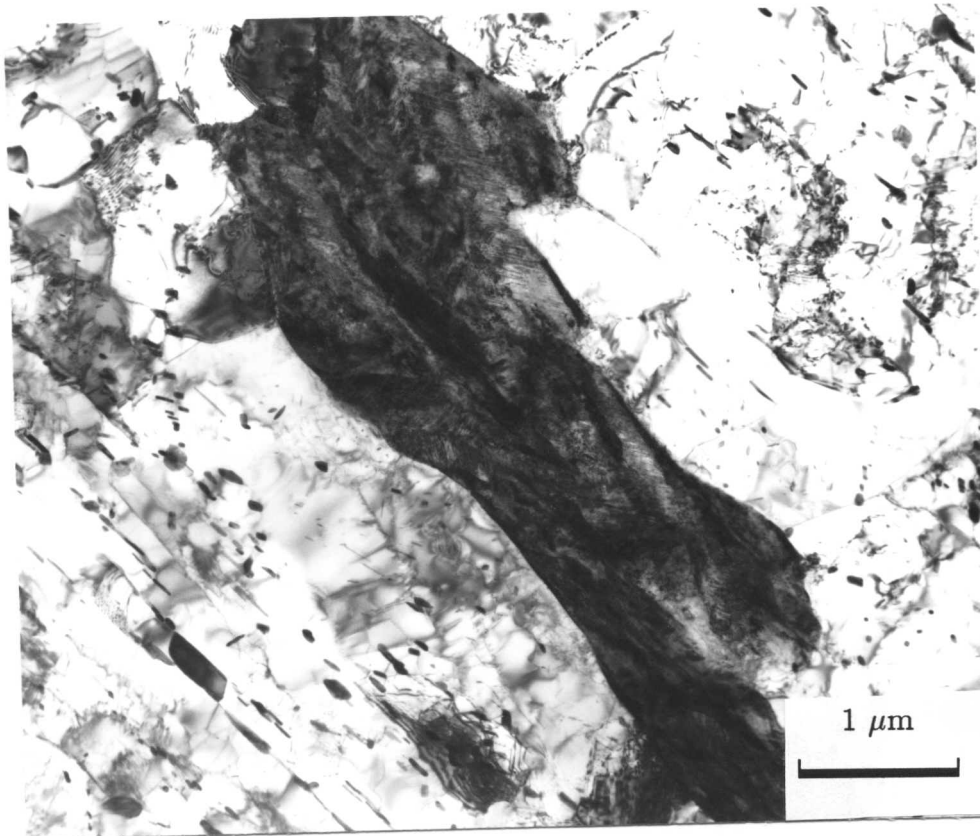


Fig. 5.15: *TEM thin foil micrographs showing that residual austenite (now converted to twinned martensite) is still left undecomposed even after 7 days of tempering at 600 °C.*

5.2.6 Effect of Tempering Time on Bulk Hardness

The hardness level dropped continuously with tempering, with no obvious secondary hardening peak due to the precipitation of carbides. On the other hand, it is likely that the softening was retarded relative to an alloy which did not contain secondary hardening element.

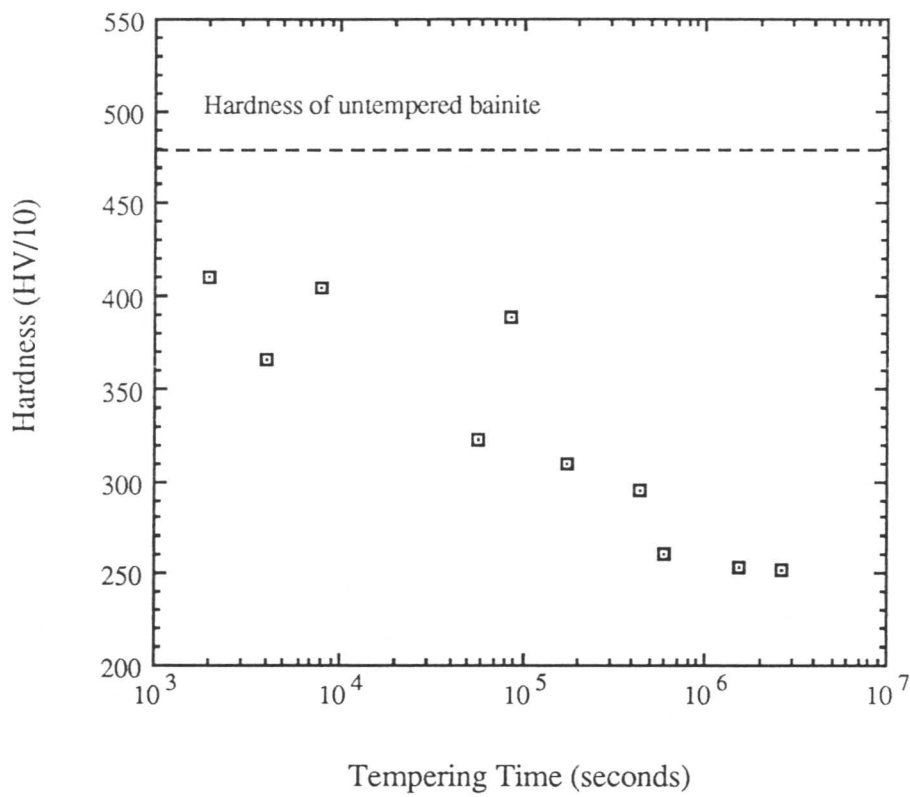


Fig. 5.16: Effect of tempering time on the bulk hardness.

5.3 Summary

Experiments have been conducted in which mixtures of bainitic ferrite and austenite were tempered at a temperature (620 °C) well above the bainite-start temperature. Annealing caused the tips of the ferrite platelets to round-off, a result which indicates that the original lenticular shape, which is a consequence of the displacive transformation mode, is not the equilibrium shape of the ferrite. The strain energy due to the shape change favours a sharp plate tip since this minimises the strain energy; annealing releases the strain, making way for the plate to adopt a shape more consistent with interfacial energy minimisation. Prolonged annealing also led to a small degree of sub-unit coalescence, the coalescence process being confined to the scale of individual sheaves since the platelets within a given sheaf are from the very beginning of transformation, interconnected. The early stages of tempering lead to the precipitation of cementite, to a small extent at the austenite grain boundaries, but mostly as a consequence of the decomposition of the films of austenite trapped between the ferrite platelets. The precipitation of cementite was eventually followed by that of Mo_2C carbides, which nucleated independently of the cementite but grew at the expense of cementite. Some M_6C carbide was also found during long term ageing. Profuse alloy carbide precipitation was eventually accompanied by the further relaxation of the ferrite grains into more equiaxed grains.



Chapter 6

EFFECT OF AUSTENITISATION TEMPERATURE ON THE FORMATION OF BAINITE

Bainite generally adopts a sheaf morphology and these sheaves usually nucleate at the prior austenite grain boundaries. These sheaves grow into the austenite grains until they are stopped by some obstacle such as an austenite grain boundary or another bainite sheaf. Prior austenite grain size can therefore be expected to play an important role in controlling the kinetics of the bainite reaction but there are contradicting results in the literature. This may partly be a consequence of the fact that complex alloy systems were used with several reactions occurring simultaneously, making the interpretation of the experimental data difficult. This chapter is devoted to the study of the effect of austenite grain size on the kinetics of bainitic transformation.

6.1 General Introduction

The usual effect of austenite grain size upon the kinetics of a grain-boundary nucleated transformation, is that of changing the number of nucleation sites per unit volume of sample. As already stated, the available data concerning the effect of austenitising temperature on the kinetics of bainite reaction are conflicting. For example Davenport and Bain [1941] found, using a Fe-0.37C-0.77Mn-0.98Cr (wt. %) steel, that the rate of bainite formation remained unaffected on increasing the austenite grain size from ASTM 7-8 to 2-3§. Similar results were obtained by Allen *et al.* [1939], who investigated the effect of increasing austenitising temperature on the isothermal transformation of a Fe-1.0Cr (wt. %) steel. They concluded that there is no detectable effect of austenitisation temperature on the subsequent formation of bainite. On the other hand, Hultgren [1947] found that in a series of Mn steels, austenitisation at higher temperatures considerably retarded the decomposition of austenite to bainite, consistent with the earlier work of Winterton [1945]. Cottrell and Ko [1953] investigated the effect of austenitising temperature on a number of Fe-Ni-Mo-Cr hypo-eutectoid low-alloy steels. For reasons which are not clear, they noticed that the rate of bainite reaction in the case of En25 and En26 is increased as the austenitising temperature was raised from 950 °C to 1300 °C, but for En31 steel there was a retardation. Graham and Axon [1953] investigated the

§ ASTM stands for American Society for Testing and Materials.

effects of austenite grain size and austenitisation temperature on the transformation to lower bainite in a Fe-0.97C wt. % alloy. It was claimed that the individual effects of grain size and austenitising temperature were separated. Specimens were austenitised for time periods ranging from 4 to 360 minutes at temperatures of 835, 900 and 990 °C and then fully reacted at 266 °C. It was found that there is an initial decrease in the decomposition rate followed by an increase, as a function of rising austenitising temperature. The initial retardation was attributed to increasing carbide solution, and the subsequent acceleration to the onset of grain growth. In further experiments specimens were austenitised at temperatures ranging from 860 to 990 °C for times chosen to ensure complete carbide solution and to establish a constant grain size of ASTM 6. It was found that the times to 5 % and 95 % reaction at 266 °C increased with increasing austenitising temperature upto about 950 °C, after which the curves flattened out. These results were taken to mean that, upon eliminating the effects due to differing grain sizes and incomplete solution of carbides, in the lower bainite range there remains an effect due to the austenitising temperature. The effect was said to be reversible in a fashion similar to that noted by Cottrell and Ko [1953], but the experimental data presented by Graham and Axon [1959] exhibit a large degree of scatter. Barford *et al.* [1961] have examined the kinetics of upper and lower bainite in Fe-Mn-C high purity steels using electrical resistivity measurements. They found that the time to any chosen percentage reaction less than 25 % is proportional directly to the mean austenite diameter.

The studies to date are not in general consistent with each other with respect to the austenitising conditions or austenite grain size dependence of the bainite transformation kinetics. This is partly because complex alloy systems were used in which the bainite reaction was sometimes accompanied by other transformations such as the precipitation of carbides or pearlite.

The present work was undertaken in order to study further the effect of austenite grain size on the bainite transformation using alloy systems in which bainitic ferrite growth occurs in isolation.

6.2 Experimental Procedures

The chemical compositions of the steels used has been given in Table 3.1, they all contain large silicon concentrations to retard the formation of carbides during bainitic transformation.

Cylindrical specimens of 3 mm diameter and 20 mm length, were prepared by

swagging and machining treatments§. All heat treatments were carried out in a Theta industries high speed dilatometer. After homogenisation at 1250 °C for 3 days, specimens were Ni-plated to prevent surface degradation during subsequent heat treatments. Fig. 6.1 shows schematically the heat treatment cycles used.

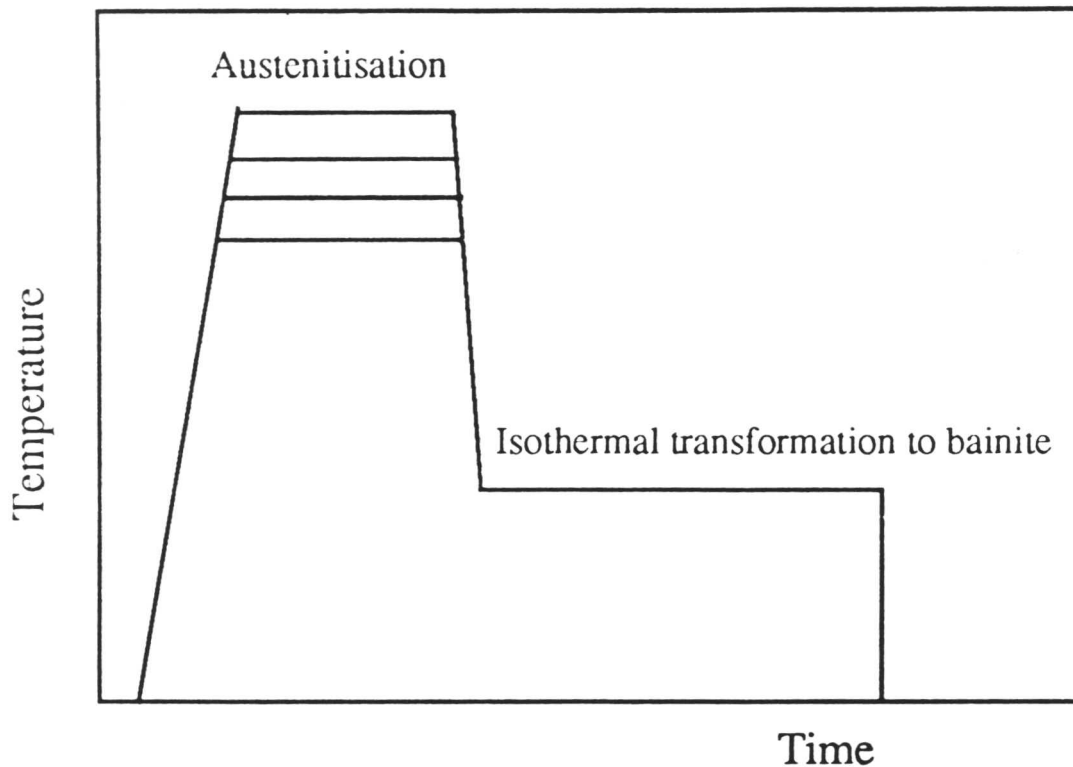


Fig. 6.1: Schematic representation of the heat treatment cycles used.

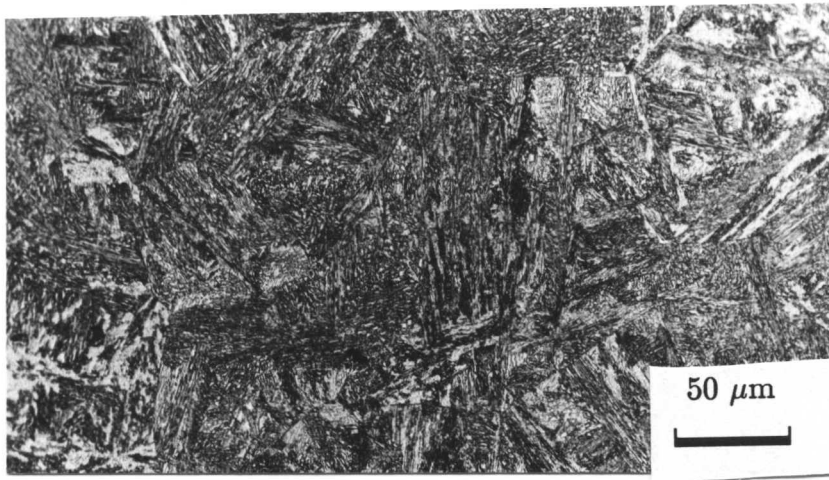
The dilatometer was interfaced with a BBC/Acorn computer for data collection. The data were subsequently transferred to an IBM 3087 main frame computer for detailed analysis according to the method described in Chapter 4. The prior austenite grain sizes were measured by sealing polished and unetched specimens in silica tubes, which were evacuated to 10^{-6} torr and sealed off under the partial pressure of dried pure argon gas. The capsules were transferred to the furnace maintained at the austenitisation temperature, austenitised for 5 min in order to thermally groove the austenite boundaries, and then air cooled to ambient temperature.

Conventional metallographic techniques were used for revealing the microstructure. The specimens were etched using 2 % nital solution.

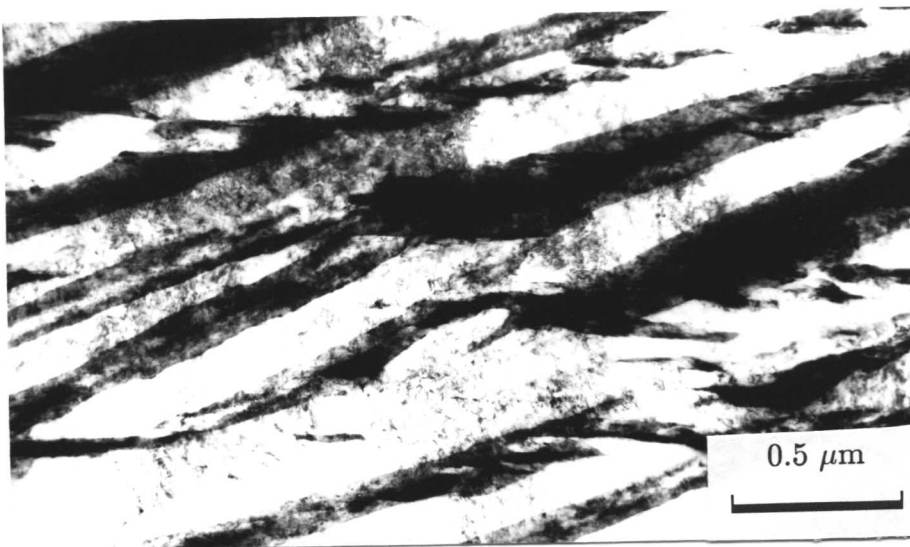
§ The details of the specimen preparation procedures are described in Chapter 3.

6.3 Results and Discussion

The micrographs in Fig. 6.2 show a typical bainitic microstructure observed in steels used in the present study. The bainite sheaves nucleate at the prior austenite grain boundaries (Fig. 6.2a) and consisted of much smaller platelets of bainitic ferrite as shown in the TEM micrograph of Fig. 6.2b. No cementite or other carbides detected in the microstructure (Fig. 6.2b).



(a)



(b)

Fig. 6.2: Micrographs showing typical bainitic microstructure in alloy A2. Specimen isothermally transformed at 400 °C for 2000 s after austenitisation at 1200 °C for 5 min. (a) Optical micrograph. (b) TEM micrograph.

6.3.1 Transformation in Alloy A2

Fig. 6.3 shows the effect of austenitisation temperature on the kinetics of the bainite reaction. The dilatometric curves indicate that the kinetics are sensitive to austenitisation temperature. In the specimens austenitised at 900 °C, the rate of transformation was found to be much higher than in those austenitised at 1200 °C.

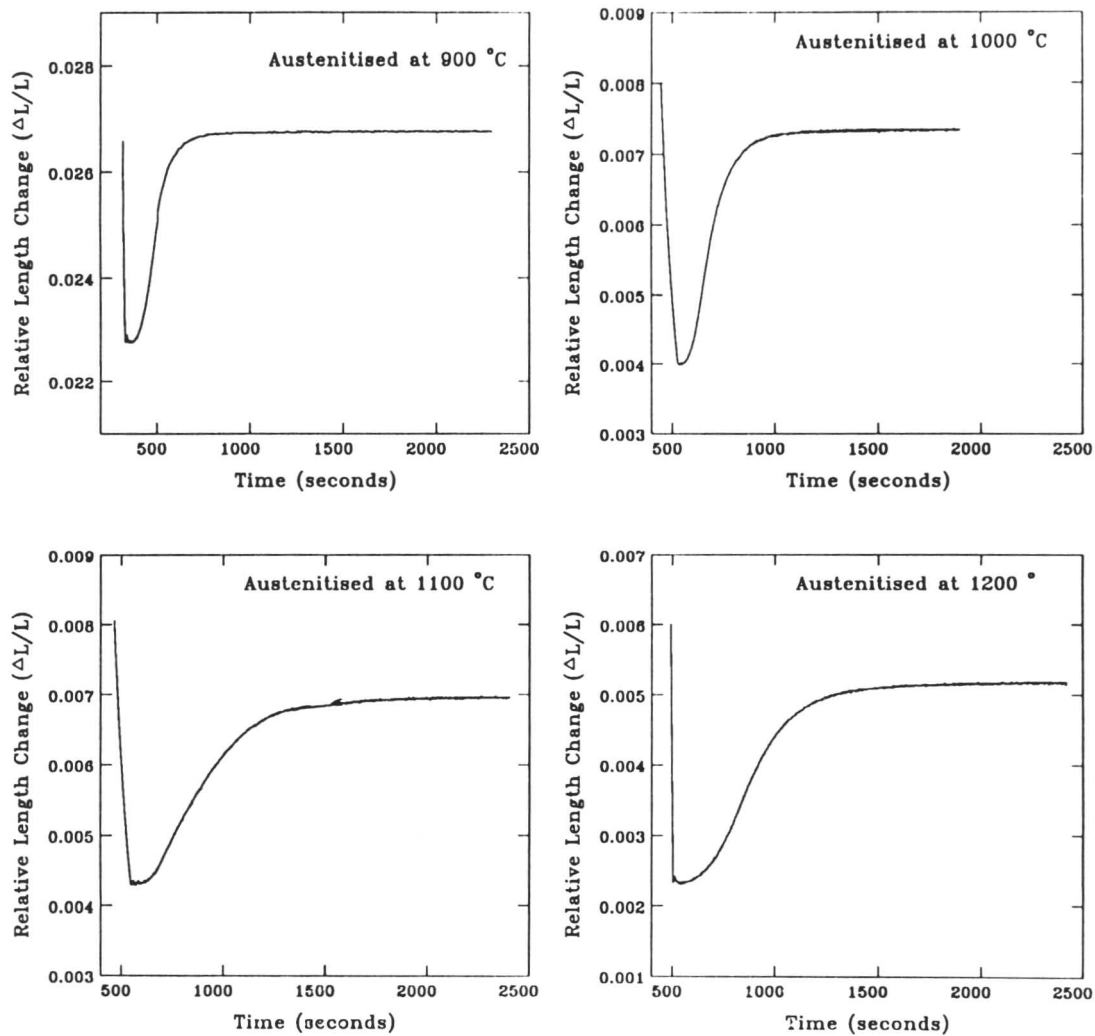


Fig. 6.3: Dilatometric curves showing the effect of austenitisation temperature on the kinetics of bainite reaction in alloy A2.